

# Cosmology with the Large Synoptic Survey Telescope: an Overview

Hu Zhan<sup>1</sup> and J. Anthony Tyson<sup>2</sup>

<sup>1</sup>CAS Key Laboratory of Space Astronomy and Technology, National Astronomical Observatories, A20 Datun Road, Chaoyang District, Beijing 100012, China

<sup>2</sup>Department of Physics, University of California, One Shields Avenue, Davis, CA 95616, USA

E-mail: zhanhu@nao.cas.cn, tyson@physics.ucdavis.edu

**Abstract.** The Large Synoptic Survey Telescope (LSST) is a high étendue imaging facility that is being constructed atop Cerro Pachón in Northern Chile. It is scheduled to begin science operations in 2022. With an 8.4 m (6.5 m effective) aperture, a novel three-mirror design achieving a seeing-limited 9.6 deg<sup>2</sup> field of view, and a 3.2 Gigapixel camera, the LSST has the deep-wide-fast imaging capability necessary to carry out an 18,000 deg<sup>2</sup> survey in six passbands (*ugrizy*) to a coadded depth of  $r \sim 27.5$  over 10 years using 90% of its observational time. The remaining 10% of time will be devoted to considerably deeper and faster time-domain observations and smaller surveys. In total, each patch of the sky in the main survey will receive 800 visits allocated across the six passbands with 30 s exposure visits.

The huge volume of high-quality LSST data will provide a wide range of science opportunities and, in particular, open a new era of precision cosmology with unprecedented statistical power and tight control of systematic errors. In this review, we give a brief account of the LSST cosmology program with an emphasis on dark energy investigations. The LSST will address dark energy physics and cosmology in general by exploiting diverse precision probes including large-scale structure, weak lensing, type Ia supernovae, galaxy clusters, and strong lensing. Combined with the cosmic microwave background data, these probes form interlocking tests on the cosmological model and the nature of dark energy in the presence of various systematics.

The LSST data products will be made available to the U.S. and Chilean scientific communities and to international partners with no proprietary period. Close collaborations with contemporaneous imaging and spectroscopy surveys observing at a variety of wavelengths, resolutions, depths, and timescales will be a vital part of the LSST science program, which will not only enhance specific studies but, more importantly, also allow a more complete understanding of the universe through different windows.

## Contents

<b>1</b>	<b>Introduction</b>	<b>2</b>
<b>2</b>	<b>Cosmological Framework</b>	<b>5</b>
2.1	Cosmic distances . . . . .	5
2.2	Growth of perturbations . . . . .	7
2.3	Two-point statistics of fluctuations . . . . .	8
<b>3</b>	<b>Cosmic Frontiers</b>	<b>10</b>
3.1	Accelerating universe . . . . .	10
3.2	Dark matter . . . . .	13
3.3	Neutrino masses . . . . .	15
3.4	Primordial perturbations . . . . .	17
<b>4</b>	<b>Large Synoptic Survey Telescope</b>	<b>17</b>
4.1	Telescope and camera . . . . .	18
4.2	Survey plan and performance . . . . .	19
4.3	Data products . . . . .	21
4.4	Engaging the community . . . . .	22
<b>5</b>	<b>LSST Probes of Cosmology</b>	<b>23</b>
5.1	Large-scale structure (BAO) . . . . .	23
5.2	Weak gravitational lensing (WL) . . . . .	26
5.3	Type Ia supernovae . . . . .	30
5.4	Galaxy clusters . . . . .	31
5.5	Strong lensing . . . . .	32
5.6	Joint analyses . . . . .	32
<b>6</b>	<b>Summary</b>	<b>37</b>

**1. Introduction**

Breakthrough discoveries have greatly expanded the boundary of our perceptible universe from the solar system to the Milky Way, to the *Realm of the Nebulae* [1], and to the afterglow of the Big Bang [2]. Tantalizing evidence for new physics from our cosmic quest calls for a new generation of powerful survey facilities. Indeed, not only do astronomers fully endorse research on the physics of the universe with long-term planning exercises such as *Cosmic Vision* [3] — the European Space Agency’s science program for 2015-2025 and *New Worlds, New Horizons in Astronomy and Astrophysics* [4] — the 2010 US Decadal Survey of Astronomy and Astrophysics (Astro2010), but physicists also fully recognize the potential to advance our fundamental understanding of the particle world through its connection with the cosmos [5, 6]. What is truly

exciting is that, after more than a decade of community efforts, ambitious projects like the Large Synoptic Survey Telescope<sup>‡</sup> (LSST) are now on track for operations starting in the early 2020s.

It was realized through early dark matter mapping experiments in the 1980s and 1990s [e.g., 7–11] that a huge survey volume was ultimately needed for useful cosmological tests with imaging surveys. Specifically, the survey should be both deep and wide. This enables precision cosmology by boosting the sample size for methods based on properties of individual objects, by suppressing the sample variance error and shot noise for methods relying on spatial statistics of the objects, and by providing information about the evolution of the universe. To complete such a survey in a reasonable time, one must resort to a facility with high étendue or “throughput”, which may be quantified by the product of the light-collecting area and the field of view (FoV) in solid angle. It would be ideally a large-aperture wide-field telescope that delivers superb image quality, which brings considerable challenges to both the optics and the camera.

The need for a high-throughput instrument for dark matter mapping motivated the Big Throughput Camera (BTC, community access started in 1996) [12, 13]. It was hosted by the National Optical Astronomy Observatory (NOAO) at the 4-meter telescope (later named Blanco telescope) at Cerro Tololo Inter-American Observatory. The BTC on the Blanco telescope had the most powerful sky survey capability at that time. The pixels critically sampled the sub-arcsecond seeing, and shift-and-stare imaging provided very deep images over moderately wide FoV. Two groups of astronomers used the BTC to search for type Ia supernovae (SNe Ia), trying to measure the expected “deceleration” of the expansion of the universe. What they found was remarkable [14, 15]: instead of decelerating, the universe is accelerating!

While the BTC could survey to  $r \sim 26$  over a few square degrees in a week, another facility using a larger mosaic of the same  $2K \times 2K$  pixel CCDs, but on a much smaller telescope, was optimized for moderate depth, very wide field observations: the Sloan Digital Sky Survey (SDSS, science operations started in 2000) [16]. The first phase of the SDSS completed in 2005, and its imaging covered  $8000 \text{ deg}^2$  of the sky in 5 bands to a depth of  $r \leq 22.2$  [17]. The SDSS has been hugely successful, broadly impacting not only astronomy but also the way research in astronomy is done. With three extensions, it has now gone well beyond its original goals.

A natural question was then whether we could meet the challenges of surveying much deeper and, at the same time, significantly wider than the SDSS. An affirmative answer in the late 1990s would seem optimistic, but progress has been made by precursors such as the Deep Lens Survey [18], the Canada-France-Hawaii Telescope Legacy Survey [19], the Panoramic Survey Telescope and Rapid Response System (Pan-STARRS) [20], and the Dark Energy Survey [21]. With a sufficiently large étendue one would not have to make choices between wide-shallow or deep-narrow surveys;

<sup>‡</sup> <http://www.lsst.org/>

one could have a facility that would do the best of both: *deep and wide*. Moreover, with a large telescope the exposures could be short, enabling a deep-wide-fast survey which could provide the data needed by a broad range of science programs from a single comprehensive set of observations. Thus was born the idea of the “Dark Matter Telescope” [22].

Plans for the wide-field Dark Matter Telescope and its camera were presented at a workshop on gravity at SLAC National Accelerator Laboratory in August 1998 [23]. The science case for such a telescope was submitted to the 2000 US Decadal Survey of Astronomy and Astrophysics (Astro2000) [24] in June 1999. This proposal emphasized the broad science reach from cosmology to the time domain through data mining of a single deep-wide-fast sky survey. Astro2000 recommended it highly as a facility to discover near-Earth asteroids as well as to study dark matter and renamed it Large-aperture Synoptic Survey Telescope (the word “aperture” is now omitted). Soon after, a summer workshop on wide field astronomy was organized at the Aspen Center for Physics in July 2001. This was the beginning of wide involvement by the scientific community in the LSST. In 2002 NOAO set up a national committee to develop the LSST design reference mission [25]. Meanwhile, plans for a multi-gigapixel focal plane and initial designs for the telescope-camera-data system were being developed [26–28].

In 2002 the National Science Foundation (NSF) funded research and development of the new CCDs required for the LSST, supplementing an investment already made by Bell Labs. L. Seppala modified R. Angel’s original three-mirror optical design for the telescope [29], creating a  $10 \text{ deg}^2$ , very low distortion FoV. The LSST Corporation was formed in 2002 to manage the project. An R&D proposal was submitted to the NSF in early 2007 and favorably reviewed later that year. Thanks to a gift from C. Simonyi and B. Gates, the LSST 8.4-m primary-tertiary mirror was cast in 2008, and in early 2009 the secondary mirror blank was cast as well.

A grass-roots effort in 2008 and 2009 by the astronomy community resulted in the *LSST Science Book* [30], a 596 page compendium of breakthrough science applications co-authored by 245 scientists. In addition, the community wrote many white papers on LSST science applications as input to the Astro2010 decadal survey process. The effort was well received, and the LSST was ranked by Astro2010 as the highest priority for ground-based astronomy [4]. In February 2011 a construction proposal was submitted to the NSF. After many project reviews, the NSF National Science Board gave approval to begin LSST construction in August 2014. The LSST construction is on schedule, and first light for engineering tests with a commissioning camera is scheduled for 2019, with the decade-long main survey beginning in 2022.

With its high étendue and image quality, the LSST is naturally a powerful facility for dark energy studies, and it will take advantage of multiple probes such as weak lensing (WL), large-scale structure (LSS), SNe Ia, galaxy clusters, and strong lensing. It is therefore classified as a Stage IV dark energy experiment, i.e., a next generation project, by the Dark Energy Task Force (DETF) [31]. These same survey data also enable related investigations such as the dark matter distribution on a variety of scales

from galaxies to the LSS and the sum of neutrino masses.

The rest of the paper is arranged as follows. Section 2 and section 3 introduce, respectively, a set of frequently encountered concepts in cosmology and several research areas that are expected to advance significantly with the LSST. We give a concise description of the LSST project in section 4 and discuss in section 5 the cosmological probes that have been developed extensively within LSST Science Collaborations. Although an emphasis is given to applications for dark energy studies, readers are reminded that these probes are sensitive to other elements of cosmology as well. For more thorough discussions of the LSST — its design, capabilities, and wide range of science opportunities, see [30]; a shorter overview is also available on the arXiv [32]. A detailed plan of the dark energy program for the LSST can be found in the white paper of the LSST Dark Energy Science Collaboration (DESC) [33].

## 2. Cosmological Framework

Modern cosmology has established a successful framework that enables precision interpretation of observational data. Such a framework is built upon Einstein’s General Relativity (GR) and the profound principle that the universe must be homogeneous and isotropic on sufficiently large scales. Clearly, alternative theories of cosmology may be constructed by modifying either GR or the cosmological principle, which are indeed areas of active studies. Nevertheless, GR plus the cosmological principle remains the most effective and self-consistent theory to date that describes the universe from its very early stage to the present. This section is hence focused on key elements of the conventional cosmological framework.

### 2.1. Cosmic distances

The Friedmann-Lemaître-Robertson-Walker (FLRW) metric [34–37] is essential for cosmology under the principle of spatial homogeneity and isotropy. The line element of the FLRW metric is given by

$$ds^2 = -c^2 dt^2 + a^2(t) \left( \frac{dr^2}{1 - Kr^2} + r^2 d\Omega \right), \quad (1)$$

where  $a(t)$  and  $K$  are the scale factor and the curvature of the universe, respectively. For convenience, the scale factor  $a(t)$  is set to unity at present time  $t_0$ . The FLRW metric is independent of GR. The influence of gravity is through the dynamics, e.g., the evolution of  $a(t)$ , so quantities and relations derived solely from the FLRW metric are often applicable to models of alternative gravity theories.

It is useful to define a distance that depends on the spatial coordinates only:

$$dD_C^2 = \frac{dr^2}{1 - Kr^2} + r^2 d\Omega. \quad (2)$$

Since the distance  $D_C$  between two bodies at rest locally in the expanding universe does not change with time, it is given the name “comoving distance.” For a photon heading

toward the observer ( $ds = d\Omega = 0$ ), the radial comoving distance along its geodesic is

$$D_C[r(t)] = \int_0^r \frac{dr'}{\sqrt{1 - Kr'^2}} = \int_t^{t_0} \frac{cdt'}{a(t')}. \quad (3)$$

With (3), one can link the observed redshift  $z$  of spectral lines of a distant object to the scale factor  $a$  at the time of emission via  $1 + z = a^{-1}$  [35]. The comoving distance between the observer and the object at  $z$  can then be written as

$$D_C(z) = \int_0^z \frac{cdz'}{H(z')}, \quad (4)$$

where the Hubble parameter  $H[z(t)] \equiv \dot{a}/a$  is a measure of the expansion rate of the universe at  $z$  (or  $t$ ), and the over-dot on  $a$  denotes derivative with respect to  $t$ . For two objects along the line of sight at  $z_1$  and  $z_2$  ( $z_2 > z_1$ ), respectively, the comoving distance between them  $D_C(z_1, z_2)$  equals  $D_C(z_2) - D_C(z_1)$ . For completeness, the time since Big Bang is given by

$$t(z) = \int_z^\infty \frac{dz'}{(1+z')H(z')}. \quad (5)$$

Two practical definitions of distances are frequently used on cosmic scales: the angular diameter distance  $d_A$  and the luminosity distance  $d_L$ . The former is the distance that converts the angular size  $\theta$  of an object into its linear size  $l$  perpendicular to the line of sight, i.e.,  $l \simeq d_A \theta$  ( $|\theta| \ll 1$ ). The luminosity distance is the radius of the sphere at which an isotropic light source with luminosity  $L$  would produce the observed flux  $F$ , i.e.,  $L = 4\pi d_L^2 F$ . By setting  $dt = dr = 0$  in (1), one can see that  $ar$  is just the angular diameter distance of the coordinate  $r$  as viewed from the origin. The integral over  $r$  in (3) can be carried out to get

$$r \equiv S_K(D_C) = \begin{cases} K^{-1/2} \sin [K^{1/2} D_C(z)] & K > 0 \\ D_C(z) & K = 0 \\ (-K)^{-1/2} \sinh [(-K)^{1/2} D_C(z)] & K < 0 \end{cases}, \quad (6)$$

so that

$$D_A(z) \equiv (1+z)d_A(z) = S_K [D_C(z)], \quad (7)$$

where  $D_A(z)$  is the comoving angular diameter distance. In lensing studies, one often needs to calculate the angular diameter distance of an object at  $z_2$  as viewed by an observer at  $z_1$  ( $z_2 > z_1$ ):

$$D_A(z_1, z_2) \equiv (1+z_2)d_A(z_1, z_2) = S_K [D_C(z_1, z_2)]. \quad (8)$$

The luminosity distance and the angular diameter distance satisfy the reciprocity relation [38] (also known as the distance-duality relation), i.e.,  $d_L(z) = (1+z)^2 d_A(z)$ . It is valid as long as [e.g., 39, 40]: (1) space-time is described by a metric theory, (2) photon geodesics are unique, and (3) photons are neither created nor destroyed along the geodesics. The reciprocity relation is therefore independent of the FLRW metric or GR, and it offers a fairly model independent test of cosmology.

## 2.2. Growth of perturbations

Gravity drives the evolution of the universe. Hence, we put GR into context here. From Einstein's field equations one can derive the Friedmann equations

$$\left(\frac{\dot{a}}{a}\right)^2 = \frac{8\pi\mathcal{G}}{3}(\rho_m + \rho_{de}) - \frac{Kc^2}{a^2} \quad (9)$$

$$\frac{\ddot{a}}{a} = -\frac{4\pi\mathcal{G}}{3}[\rho_m + \rho_{de}(1 + 3w_{de})], \quad (10)$$

where  $\mathcal{G}$  is the gravitational constant,  $\rho_m$  is the matter density<sup>§</sup>,  $\rho_{de}$  is the dark energy density,  $w_{de}$  is the dark energy equation of state (EoS), and we have neglected the radiation component as well as the pressure of matter. Equation (10) shows that  $w_{de} < -1/3$  is a necessary (but not sufficient) condition for dark energy to drive the cosmic acceleration ( $\ddot{a} > 0$ ). Conservation of energy leads to a generic scaling

$$\rho_x(z) = \rho_x(0) \exp\left[3 \int_0^z \frac{1 + w_x(z')}{1 + z'} dz'\right], \quad (11)$$

where the subscript  $x$  can be “m” or “de.” Since the EoS of matter  $w_m$  is practically zero in the redshift range directly observed by the LSST, we can drop the subscript “de” in  $w_{de}$  without confusion. Equation (9) can now be rewritten as

$$\frac{H^2(z)}{H_0^2} = \Omega_m(1+z)^3 + \Omega_k(1+z)^2 + \Omega_{de} \exp\left[3 \int_0^z \frac{1 + w(z')}{1 + z'} dz'\right], \quad (12)$$

where  $H_0 \equiv H(0)$  is the Hubble constant,  $\Omega_m \equiv \rho_m(0)/\rho_c$  with  $\rho_c \equiv 3H_0^2/(8\pi\mathcal{G})$ ,  $\Omega_k \equiv -Kc^2/H_0^2$ , and  $\Omega_{de} \equiv \rho_{de}(0)/\rho_c = 1 - \Omega_m - \Omega_k$ . If dark energy is just the cosmological constant  $\Lambda$  ( $w = -1$ ),  $\rho_{de}$  indeed will be a constant over time. A flat universe dominated by the cosmological constant and cold dark matter (CDM) is often referred to as the  $\Lambda$ CDM universe, and we use  $w$ CDM to denote the case  $w \neq -1$ . Equation (12) shows that  $H_0$ ,  $\Omega_m$ ,  $\Omega_{de}$  (or  $\Omega_k$ ), and  $w(z)$  completely specify the cosmic expansion history, which, in turn, determines the distances and time defined in section 2.1.

Gravitational instability turns minute initial fluctuations into structures we observe today. The growth history of these fluctuations provides crucial cross-checks of the cosmological model. On linear scales, the overdensity of the perturbed density field  $\rho_m(\mathbf{x}, t)$  can be decomposed into a spatial component and a time component

$$\delta_m(\mathbf{x}, t) \equiv \frac{\rho_m(\mathbf{x}, t) - \rho_m(t)}{\rho_m(t)} = \delta_m(\mathbf{x})G(t), \quad (13)$$

where  $G(t)$  is the linear growth function. Assuming that dark energy does not cluster on scales of interest, one obtains for the fluctuations in matter

$$\ddot{G} + 2H\dot{G} = 4\pi\mathcal{G}\rho_m G. \quad (14)$$

It can be seen that the Hubble expansion in (14) works against gravity, so the cosmic acceleration slows down the growth of structures. Gravity in general affects both the

<sup>§</sup> Including both ordinary matter and dark matter. The former is often referred to as baryons in astronomy for convenience.

Hubble expansion and the right-hand side of (14). Therefore, one can potentially distinguish dark energy from modified gravity theories by examining both the expansion history (or distances) and the growth history of the universe [e.g., 41–43] *if* dark energy is completely homogeneous and isotropic.

In analyses of galaxy redshift surveys, one often needs the logarithmic growth rate

$$f(z) = \frac{d \ln G}{d \ln a} \approx [\Omega_m(z)]^\gamma, \quad (15)$$

where the growth index  $\gamma \sim 0.55\text{--}0.6$  is not overly sensitive to cosmological parameters within the GR framework [44–47].

### 2.3. Two-point statistics of fluctuations

Statistics of the cosmic density field are crucial probes of the universe. In the linear regime, the cosmic density field can be approximated by a Gaussian random field, whose properties are all captured in its two-point statistics, i.e., the correlation function in configuration space or, equivalently, the power spectrum in Fourier space. For this reason, we discuss only the two-point statistics here. For higher-order statistics and their applications, see, e.g., [48–50].

The correlation function of the overdensity  $\delta(\mathbf{x})$  is defined as

$$\xi(\Delta x) = \langle \delta(\mathbf{x})\delta(\mathbf{x}') \rangle, \quad (16)$$

where  $\langle \dots \rangle$  denotes an ensemble average, and, because of isotropy, the correlation function depends only on the separation  $\Delta x = |\mathbf{x}' - \mathbf{x}|$  between two points. Under the assumption of homogeneity and ergodicity, one can conveniently replace the ensemble average in (16) with a volume average. Real observations are made on the past light-cone, not on a snapshot (i.e., a constant-time hypersurface) of the universe, so the volume average of the light-cone differs slightly from that of the snapshot, which is seen in  $N$ -body simulations [51, 52]. Such an effect is deterministic and can be precisely calibrated.

The distribution of galaxies may differ from that of matter. A clustering bias is thus introduced to account for the difference between the galaxy correlation function  $\xi_g$  and the matter correlation function, i.e.,  $\xi_g = b^2\xi$ . The galaxy bias evolves with time and depends on the halo mass [53–56]. It also varies with the scale but changes rather slowly above tens of  $h^{-1}\text{Mpc}$  [e.g., 57, 58]. While the galaxy bias is a complex subject of research [see 59–62, for early theoretical investigations], we treat it as a constant for simplicity. In analyses of galaxy clustering data, it is useful to model the galaxy bias in detail, so that one can extract cosmological information from small scales [63–65].

The correlation of the Fourier modes  $\hat{\delta}(\mathbf{k})$  defines the power spectrum  $P(k)$

$$\langle \hat{\delta}(\mathbf{k})\hat{\delta}^*(\mathbf{k}') \rangle = (2\pi)^3 \delta^D(\mathbf{k} - \mathbf{k}')P(k), \quad (17)$$

where  $\delta^D(\mathbf{k} - \mathbf{k}')$  is the Dirac delta function. The power spectrum is often expressed in a dimensionless form  $\Delta^2(k) = k^3 P(k)/2\pi^2$ , which is roughly the amplitude of fluctuations

in the logarithmic interval around  $k$ . By Fourier expanding  $\delta(\mathbf{x})$  in (16), one finds that the correlation function in configuration space is just the Fourier transform of  $P(k)$ , i.e.,

$$\xi(\Delta x) = \frac{1}{(2\pi)^3} \int e^{i\mathbf{k}\cdot\mathbf{x}} P(k) d^3k. \quad (18)$$

Real surveys have finite volume and resolution, so one applies the discrete Fourier transform in practice. Since the power spectrum and the correlation function are equivalent, data analyses can be performed with either statistic. Still, the complexity of the analyses depends on both the adopted statistic and the application. Besides the multiplicative galaxy bias, the galaxy power spectrum receives an additive term due to the shot noise

$$P_g(k) = b^2 P(k) + n_g^{-1}, \quad (19)$$

where  $n_g$  is the galaxy number density. The galaxy bias in (19) is equivalent to that in the galaxy correlation function *if* it is scale-independent.

The statistical error of the power spectrum at the wavevector  $\mathbf{k}$  equals the power spectrum itself, i.e.,  $\sigma_{P_g}(\mathbf{k}) = P_g(k)$  [66]. The errors at different wavevectors are independent under a Gaussian approximation, so the uncertainty of a band power can be reduced effectively

$$\sigma_{P_g}(k) = \sqrt{\frac{2}{N_k}} P_g(k), \quad (20)$$

where  $N_k$  is the number of modes within a band of width  $\Delta k$ . For a survey of volume  $V$ ,  $N_k \simeq k^2 \Delta k V / 2\pi^2$ . The uncorrelated errors make the power spectrum convenient for at least theoretical studies. With observational effects and nonlinearity, one can still decorrelate the modes with some effort [67, 68].

In the linear regime, where  $\Delta^2(k) \ll 1$ , all the modes grow at the same rate with no coupling to each other. Therefore, the linear power spectrum at a redshift well below the redshift of the cosmic microwave background (CMB,  $z \sim 1100$ ) can be scaled from that at a reference redshift (e.g.,  $z = 0$ ) using the linear growth factor

$$P_L(k, z) = \frac{G^2(z)}{G^2(0)} P_L(k, 0). \quad (21)$$

Because of the complex nature of the galaxy bias, it is not straightforward to predict the galaxy power spectrum precisely. One usually has to fit the galaxy bias parameter(s) with data. However, it is encouraging that relatively simple bias models based on the concept of halos [62, 69, 70] are largely consistent with current observations [71–74].

Perturbative calculations can extend the power spectrum prediction into the weakly nonlinear regime [75–81]. Going further, one must resort to cosmological  $N$ -body simulations. Tests with simulations have reached 1% level accuracy out to  $k \sim 1 h\text{Mpc}^{-1}$  [82], which is within a factor of a few from the requirements of future surveys [83, 84]. However, the cost of running  $N$ -body simulations makes them impractical for direct use in cosmological parameter estimation. A solution to this problem is in essence to develop an advanced interpolation scheme that can quickly output the power spectrum

with satisfactory accuracy from a minimum set of simulations spanning the parameter space [85–88]. For less demanding applications, fitting formulae for the nonlinear matter power spectrum [89–91] are convenient to use.

### 3. Cosmic Frontiers

Cosmology is a key science driver of the LSST. Although great discoveries often come unexpected, there are many areas for which one can predict substantial progress with the LSST. Here we give a brief account of several such areas.

#### 3.1. Accelerating universe

The cosmic acceleration is undoubtedly a profound challenge to our understanding of the universe [5, 6, 31]. So far investigations have been focused on two classes of models: dark energy and modified gravity [for recent reviews, see 92–94]. The former is developed under the framework in section 2 as a special component of the universe, while the latter induces the acceleration with a new form of gravity. There are also models that admit no new components or physics but attribute the acceleration to a breakdown of the cosmological principle or an oversimplification of GR effects in the real universe [e.g., 95–97]. These models are less popular, but they do invite a closer inspection of the cosmological framework and the evidence for the cosmic acceleration.

Consider SNe Ia as an example. One may fit their luminosity distances with a Friedmann model in section 2.2, and the acceleration can be deduced from the resulting model parameters. Because the result is obtained under a model that allows acceleration in the first place, it is hard to draw a definitive conclusion before exhausting all other possibilities. Alternatively, one can estimate the deceleration parameter — a kinematic quantity

$$q = -\frac{a^2 \ddot{a}}{\dot{a}^2 a} = \frac{d \ln H}{d \ln(1+z)} - 1 \quad (22)$$

without referring to the dynamics [98, 99]. Studies along this line indeed show that  $q < 0$ , i.e.,  $\ddot{a} > 0$ , at low redshift [100–102]. Since  $\ddot{a}$  involves the second derivative with respect to time, measurements of the cosmic time or age of the universe at a series of redshifts would give the most direct evidence. However, such measurements are rather challenging. For example, the redshift drift effect can map the evolution of the cosmic expansion rate in theory [103, 104]. But even if one could monitor an object’s redshift stably over decades to measure a  $\sim 10^{-9}$  change in its redshift, peculiar velocities and other uncertainties associated with the object itself could easily dominate over the signal [105, 106]. A more practical example is to measure the cosmic expansion rate from age differences of passively evolving galaxies [107]. This technique has achieved typical precision of 5–14% on the Hubble parameter up to  $z \sim 1$  [108], though further improvement is needed to quantify the acceleration precisely via (22).

A negative deceleration parameter signifies acceleration in an FLRW universe. If, however, the cosmological principle does not hold, then one cannot use a global scale factor like that in the FLRW metric to describe the expansion of the universe. Consequently, the deceleration parameter, if measurable at all, becomes a local quantity, and a local acceleration does not necessarily mean a global acceleration of the universe. This is the case for models which place the observers in an accelerating void [109–111], which are however in tension with the data [112, 113]. In addition, nonlinear evolution of small-scale inhomogeneities have been postulated to cause an apparent acceleration on much larger scales [95, 114–117]. Although such an effect is found to be negligible [118–120], the question about the validity of the FLRW metric for interpreting real observations is highly relevant and deserves careful examination.

Applying the FLRW metric with GR, one finds that a smooth component with strong negative pressure, i.e., dark energy, is needed to drive the accelerated expansion. Its simplest form, the cosmological constant  $\Lambda$ , was invented by Einstein nearly a century ago to keep the universe static. Decades before the SN Ia results in 1998, many had already argued for a positive cosmological constant based on a range of observations including the LSS, CMB, Hubble constant, and so on [121–125]. Even a time-varying cosmological “constant” due to a scalar field was proposed by Peebles & Ratra in 1988 [126]. Depending on the behavior of the scalar field’s kinetic and potential terms, one arrives at the quintessence model ( $-1 < w < 1$ ) [127], the phantom model ( $w < -1$ ) [128], and the quintom model ( $w$  can cross  $-1$  with the help of two fields) [129]. Many more dark energy models have been discussed in the literature, and interested readers are referred to [130] for a review.

Phenomenologically, dark energy is characterized by its present energy density as a fraction of the critical density  $\Omega_{\text{de}}$  and its EoS  $w$ . A major task of dark energy experiments is thus to measure  $\Omega_{\text{de}}$  and reconstruct  $w$  as a function of redshift for model comparison. A widely used parametrization of the EoS is  $w = w_0 + w_a(1 - a)$  [131, 132]. The reciprocal of the area of the  $w_0$ - $w_a$  error ellipse was introduced as a figure of merit by the DETF [31] to evaluate the performance of various surveys<sup>||</sup>. To fully utilize the capability of future surveys (so-called Stage IV dark energy experiments), one should go beyond the  $w_0$ - $w_a$  parametrization [133, 134].

Besides strong negative pressure, dark energy might also have a sound speed that is sufficiently low to allow appreciable clustering on very large scales. The sound speed of standard quintessence is equal to the speed of light, while models such as  $k$ -essence [135] can produce a sound speed well below the speed of light over certain period of time [136]. The effect of dark energy clustering might be detected with CMB and galaxy surveys on very large scales [137, 138].

Modified gravity offers another mechanism to drive the cosmic acceleration. There are two well studied models: Dvali-Gabadadze-Porrati (DGP) gravity [139] and  $f(R)$  gravity [140, 141]. In the DGP model, matter is confined in a 4-dimensional brane, while

<sup>||</sup> The report uses the 95% confidence limit, i.e., roughly  $2\sigma$  in the Gaussian case, to define the error ellipse, but studies afterward frequently use the 68.3% confidence limit ( $1\sigma$ ) instead.

gravity can leak into the fifth dimension above a transition scale  $r_c$ , causing it to weaken faster than expected in a 4-dimensional space-time. The  $f(R)$  model replaces the Ricci scalar  $R$  in the GR gravitational action with a function  $f(R)$ . A suitable choice of  $f(R)$  could accelerate the cosmic expansion. Unfortunately, neither model appears viable. On the one hand, DGP gravity is inconsistent with observations [142]. On the other hand,  $f(R)$  gravity is constrained to be so close to GR that dark energy is still needed to drive the acceleration [143]. Nonetheless, it is useful to see from a specific example how to generate the accelerated expansion. Hence, we include a few equations of the DGP model here. The Friedmann equation becomes [144]

$$H^2 - \epsilon \frac{c}{r_c} \sqrt{H^2 + \frac{Kc^2}{a^2}} = \frac{8\pi\mathcal{G}}{3} \rho_m - \frac{Kc^2}{a^2}, \quad (23)$$

where  $\epsilon = \pm 1$ . An acceleration in the DGP model is produced with  $\epsilon = +1$ . The linear growth function satisfies [145]

$$\ddot{G} + 2H\dot{G} = 4\pi\mathcal{G} \left(1 + \frac{1}{3\beta}\right) \rho_m G, \quad (24)$$

where

$$\beta = 1 - 2\frac{Hr_c}{c} \left(1 + \frac{\dot{H}}{3H^2}\right). \quad (25)$$

Comparing with the corresponding equations in GR, one sees that DGP gravity (and modified gravity in general) affects the linear growth by altering both the expansion background, i.e.,  $H$  on the left-hand side of (24), and the effective strength of gravity on the right-hand side.

Distinguishing dark energy from modified gravity is of particular interest, as the physics behind them are fundamentally different. If dark energy only affects the background expansion, then one may detect the signature of modified gravity from inconsistency between the expansion history and the growth history. With more generic (parametrizations of) dark energy and modified gravity models, the task is thought to be impossible [146, 147], though it may still be feasible for dark energy models with no coupling to matter [148].

Redshift evolution of the Hubble parameter, angular diameter distance, linear growth function, and growth rate are shown in figure 1 for five cosmological models. The parameters of the  $\Lambda$ CDM model adopt *Planck* 2015 results [149]. The  $w$ CDM1 and  $w$ CDM2 models differ from the  $\Lambda$ CDM model only in the dark energy EoS. It is relatively easy to tune different models to match either the expansion or the growth history, but not so easy to match both. For instance, whereas the  $w$ CDM1 model is practically indistinguishable from the DGP2 model in terms of  $D_A(z)$  and  $H(z)$ , the differences in  $G(z)$  and  $f(z)$  are conspicuous. Although the  $w$ CDM2 model coincides with the  $\Lambda$ CDM model in  $G(z)$  and  $f(z)$ , measurements of  $D_A(z)$  and  $H(z)$  to better than 1% at multiple redshifts below  $z \sim 2$  can tell them apart. A similar case occurs between the DGP1 and the DGP2 models.

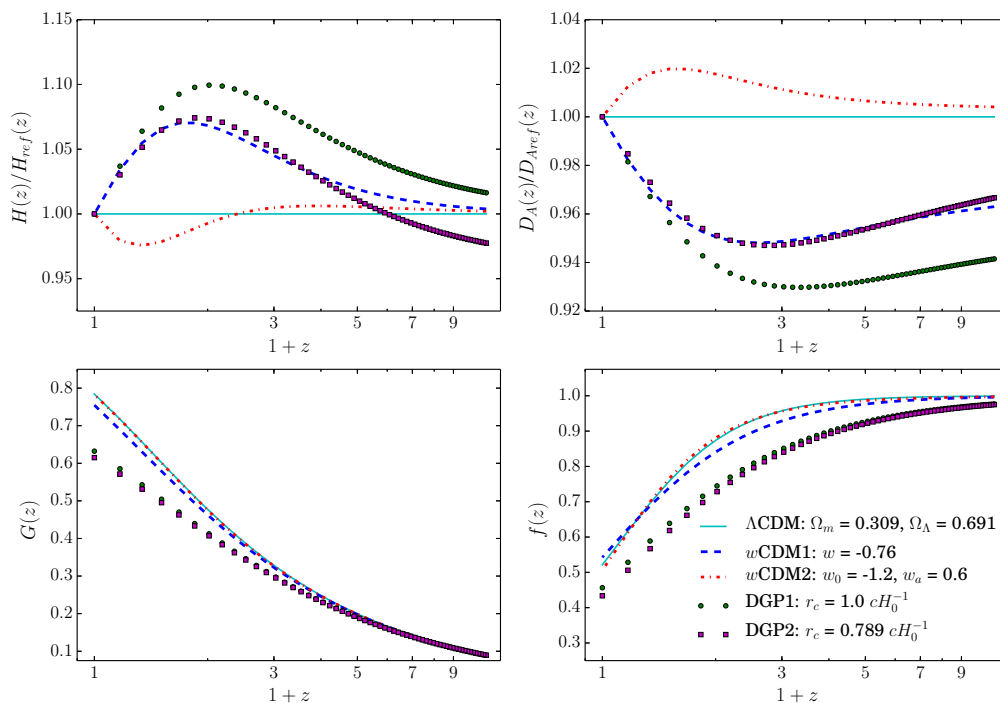


**Figure 1.** Upper left panel: Hubble parameter of various models relative to that of the  $\Lambda$ CDM model with  $\Omega_m = 0.309$  (solid line). The models are  $w$ CDM1 with  $w = -0.8$  (dashed line),  $w$ CDM2 with  $w_0 = -1.2$  and  $w_a = 0.6$  (dot-dashed line), DGP1 with  $r_c = cH_0^{-1}$  (circles), and DGP2 with  $r_c = 0.789cH_0^{-1}$  (squares). All models are flat. Upper right panel: same as the upper left panel but for the angular diameter distance. Lower left panel: linear growth factor of all the models. Lower right panel: growth rate of all the models.

Figure 1 clearly demonstrates the value of accurately mapping both the expansion history and the growth history of the universe. The Hubble parameter and different types of distances allow us to distinguish the  $\Lambda$ CDM model from dynamical dark energy models, while the growth function and growth rate are useful for breaking the degeneracy between modifications to gravity and the background expansion effect. Note that spectroscopic surveys are needed to measure  $H(z)$  and  $f(z)$  from radial baryon acoustic oscillations (BAOs) [150–154] and the redshift distortion effect [155–158], respectively. Future imaging and spectroscopic surveys will be able to constrain the quantities in figure 1 to the percent level in many redshift bins up to  $z \lesssim 3$  [159–161], which is sufficient to distinguish models with even smaller differences than those shown.

### 3.2. Dark matter

Dark matter is another major frontier of cosmology and particle physics and has a much longer history of study than dark energy. The existence of dark matter is evidence for physics beyond the standard model. Astrophysical evidence for the existence of dark matter comes from many directions including, for example, dynamics of galaxy clusters, galaxy rotation curves, X-ray emissions from galaxies and clusters, and WL

mass mapping [162–167]. Formation of galaxies and substructures within them requires dark matter, or at least the main component of it, to have a low velocity dispersion (hence “cold”) in the early universe [168]. Out of the diverse topics in dark matter research, we can only touch upon a few that are relevant to the LSST. Readers are referred to [169, 170] for thorough reviews.

Optical observations are crucial to dark matter studies that probe its gravitational effects. An important application is to determine the mean density parameter of dark matter  $\omega_{\text{dm}} = \Omega_{\text{dm}} h^2$  (equivalent to  $\rho_{\text{dm}}$ ; ditto matter density  $\omega_{\text{m}}$  and baryon density  $\omega_{\text{b}}$ ) or its fraction  $\Omega_{\text{dm}}$  in the total matter-energy budget of the universe. One can estimate  $\Omega_{\text{dm}}$  in a number of ways. Distance measurements can constrain the total matter fraction  $\Omega_{\text{m}}$ , which is the sum of  $\Omega_{\text{dm}}$  and  $\Omega_{\text{b}}$  (neglecting radiation and other minor components), and then  $\Omega_{\text{dm}}$  can be obtained with a prior on  $\Omega_{\text{b}}$ , which might also be deduced from the same survey data. Sensitivity of the abundance of massive halos and its evolution to  $\Omega_{\text{m}}$  (in combination with the normalization of density fluctuations  $\sigma_8$ ) provides another way to determine  $\Omega_{\text{dm}}$  [171]. One can also estimate  $\Omega_{\text{dm}}$  and  $\Omega_{\text{b}}$  from the shape of the matter power spectrum. So far, analyses of the CMB power spectra have obtained the most precise results on these parameters [149, 172]. Surveys like the LSST will eventually achieve similar or greater statistical power than analyses of the CMB do and will enable significant improvement over CMB-only results [173, 174].

The left panel of figure 2 illustrates the difference between two  $\Lambda$ CDM models with  $\omega_{\text{dm}} = 0.119$  [149] and  $\omega_{\text{dm}} = 0.137$  (15% higher than the former), respectively. The reduced Hubble constant takes the value of  $h = 0.677$  for both models. The power spectra are calculated using CLASS [175]. Note that the shape of the matter power spectrum depends on  $\omega_{\text{dm}}$  and  $\omega_{\text{b}}$  rather than  $\Omega_{\text{dm}}$  and  $\Omega_{\text{b}}$  and that the different values of  $\Omega_{\text{m}}$  in the two models cause a slight mismatch between their linear growth functions. The power spectra at  $z = 0$  are normalized at  $k = 0.02 \text{ Mpc}^{-1}$ . The prominent turnover feature around  $k_{\text{eq}} \simeq 0.016 h \text{ Mpc}^{-1}$  is related to the epoch of matter-radiation equality ( $a_{\text{eq}} \simeq 2.8 \times 10^{-4}$ ). In the radiation era, i.e.,  $a < a_{\text{eq}}$ , perturbations within the horizon were frozen. Smaller-scale perturbations entered the horizon earlier and experienced more suppression. After matter became dominant, perturbations of all scales evolved identically until nonlinearity or non-gravitational interactions became important. A higher matter density means that the matter-radiation equality occurred at an earlier time when the horizon was smaller. Therefore, the turnover scale shifts to a smaller scale (larger  $k$ ) with a higher  $\omega_{\text{dm}}$  if  $\omega_{\text{b}}$  remains the same. In terms of parameter estimation, scales below the turnover generally provide stronger constraints. The wiggles around  $k \sim 0.1 h \text{ Mpc}^{-1}$  in the power spectra are the BAO feature arising from the perturbations in the same cosmic fluid that produced the CMB [176–178]. It is an important cosmological probe as discussed in section 5.1.

The mean density of dark matter in the universe is only one piece of the puzzle. More information is needed to decipher the physics of dark matter. Despite its success on cosmological scales, the CDM paradigm is at odds with observations on galactic and smaller scales, which have been phrased as the missing satellite problem (too many

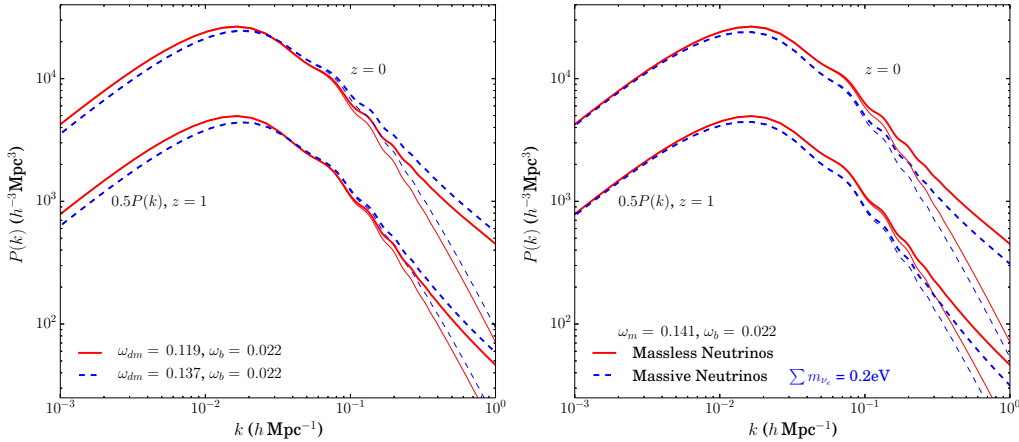


**Figure 2.** *Left:* Linear (thin lines) and nonlinear (thick lines) matter power spectra of two  $\Lambda$ CDM models with  $\omega_{\text{dm}} = 0.119$  (solid lines) and  $\omega_{\text{dm}} = 0.137$  (dashed lines). *Right:* Same as left, but the  $\omega_{\text{dm}} = 0.137$  model is replaced by a model with massive neutrinos ( $\sum m_{\nu_i} = 0.2 \text{ eV}$ ). The two models share the same matter density of  $\omega_{\text{m}} = 0.141$ .

subhalos in simulations than observed) [179, 180] and the cusp-core problem (halos’ central dark matter profile much shallower than predicted) [181–184]. There is also a related “too big to fail” problem (mismatch between massive subhalos in Milky Way-like simulations and the observed bright satellites of the Milky Way) [185]. Two routes to resolve the issues have been pursued: one is to investigate baryonic processes, such as star formation and energetic feedback, that may lead to the observed properties of dark matter structures [186], and the other tries to match the observations by replacing CDM with, for example, warm dark matter, self-interacting dark matter, or nonthermally produced dark matter [187–189]. Both approaches need full development to establish a sound connection between dark matter theories and observations, which will be indispensable for proper interpretations of dark matter particle experiments as well. Besides studies of galaxies and their satellites, the small-scale dark matter power spectrum probed by quasar spectra (known as the Ly $\alpha$  forest) and the local dark matter density measured from the stellar distribution and kinematics will also provide vital information about the physics of dark matter [e.g., 190, 191]. In rare merging systems such as the Bullet cluster [192], galaxies and dark matter may be separated from the hot X-ray gas. Based on the separation, kinematics, and other information, one can place a limit on the dark matter self-interaction cross-section [193, 194]. The LSST and other facilities together will greatly expand the samples for dark matter studies and bring more insights with precision measurements.

### 3.3. Neutrino masses

Unlike dark energy and dark matter, neutrinos are part of the standard model of particle physics, but the non-vanishing mass of at least one neutrino species still needs explanation. Astronomical observations are crucial for determining the sum of

neutrino masses ( $\sum m_{\nu_i}$ , sum over three families) [149, 172, 195, 196]. With neutrino oscillation results, the individual neutrino masses can be determined up to an ambiguity between the normal hierarchy (one species much heavier than the other two) and the inverted hierarchy (one species much lighter than the other two) [e.g., 197]. If  $\sum m_{\nu_i}$  is constrained to less than 0.1 eV, then the inverted hierarchy would be disfavored [198]. An accuracy of better than 0.02 eV is needed at  $\sum m_{\nu_i} = 0.06$  eV to exclude the inverted hierarchy at more than 95% confidence level [199].

The *Planck* limit on  $\sum m_{\nu_i}$  with CMB, BAO, SN Ia, and  $H_0$  data is 0.23 eV (95%) for a  $\Lambda$ CDM universe [149], which is somewhat sensitive to datasets combined as well as model assumptions. A more recent analysis tightens the bound to an interesting regime of  $\sim 0.1$  eV [200]. The results indicate that the neutrinos decoupled from other matter before matter-radiation equality and became non-relativistic, i.e., matter-like, during matter domination. In this scenario, the matter-radiation equality is slightly delayed compared to that with massless neutrinos (assuming the same total matter density). Perturbations entering the horizon before the transition thus have slightly less time to grow, while those afterward are not affected. Well below their free-streaming scale, the neutrinos do not contribute to overdensities, but they are still counted toward the mean matter density. Therefore, small-scale density perturbations continue to be suppressed after the neutrinos' non-relativistic transition. The overall suppression of the matter power spectrum relative to that with massless neutrinos reaches a constant factor of approximately  $\Delta P/P \simeq -8f_\nu$  at  $k \gtrsim 5 h\text{Mpc}^{-1}$  for  $f_\nu \lesssim 0.07$  [201], where  $f_\nu$  is the mean fraction of neutrinos in matter. The effect on intermediate scales requires detailed calculations [e.g., 202].

The right panel of figure 2 compares the matter power spectra of the  $\Lambda$ CDM models with massless and massive neutrinos, respectively. For  $\sum m_{\nu_i} = 0.2$  eV, the non-relativistic transition would occur at  $a_{\text{nr}} = 7.5 \times 10^{-3}$ , corresponding to a scale of  $k_{\text{nr}} = 4.5 \times 10^{-3} h\text{Mpc}^{-1}$ . Figure 2 indeed shows that the matter power spectra at  $k \lesssim k_{\text{nr}}$  are not affected by the neutrino masses. The shift of the turnover scale is barely discernible, and the suppression of the power spectra on small scales is pronounced. Nonlinear evolution appears to amplify the suppression effect of the neutrino masses. However, the nonlinear matter power spectra are calculated using the fitting formula from [90], which does not include massive neutrinos. Simulations are needed to obtain more accurate results with massive neutrinos [203, 204], and care must be taken to properly setup the initial conditions [205].

Besides the sum of neutrino masses, astronomical observations also have sensitivity to the number of neutrino species  $N_\nu$  (or the effective number of radiation components  $N_{\text{eff}}$ ). Forecasts with ideal assumptions predict that future surveys will reduce the uncertainties to roughly 0.02 eV on  $\sum m_{\nu_i}$  and 0.05 on  $N_{\text{eff}}$  [198, 206, 207]. Therefore, it is within the statistical capability of these surveys to determine the sum of neutrino masses given the minimum possible value of  $\sum m_{\nu_i} \sim 0.06$  eV and to positively detect extra neutrino or radiation species. The challenge is to disentangle neutrino effects from those of other astrophysical and observational factors such as the galaxy bias and

systematics.

### 3.4. Primordial perturbations

Previous subsections have shown the importance of the density fluctuations for determining the composition of the universe, though the origin of the fluctuations remains to be addressed. A generic prediction of inflationary models is that quantum fluctuations in the inflaton — a scalar field that drove inflation — seeded the density fluctuations today [e.g., 208]. Inflaton perturbations were stretched outside the horizon during inflation and reentered the horizon afterward as metric perturbations, which became initial conditions of the density fluctuations. The primordial metric perturbations are nearly scale invariant, so that the corresponding initial matter power spectrum  $P(k) \propto k^{n_s}$  with the power spectral index  $n_s \sim 1$ . A small departure of  $n_s$  from unity is due to the slowly varying Hubble parameter and the inflaton field during inflation. Besides the inflaton perturbations, gravitational waves generated during inflation induce B-mode polarization in the CMB [209, 210], which have been vigorously pursued by a number of experiments [211–213].

The primordial perturbations are of great interest for studies of inflation. Evolution of the second-order perturbations after inflation always produces some amount of non-Gaussianity, which is quantified by  $f_{\text{NL}}$  — a coefficient of the second-order term in the gravitational potential. A null detection at the level of  $f_{\text{NL}} \sim 1$  would rule out the standard cosmological model [e.g., 214]. As mentioned in section 3.2, physics within the horizon has altered the perturbations that reentered the horizon before the matter-radiation equality; only very large-scale modes are unaffected. Therefore surveys of huge volumes are necessary to infer the primordial perturbation spectrum and to probe the physics in the inflation era. CMB experiments have made remarkable achievements in this area [e.g. 215, 216], though these results are based on a two-dimensional projection of three-dimensional modes. The LSST and other surveys will enable studies of the primordial perturbations with a comparable statistical power based on galaxy statistics in a huge three-dimensional volume [173, 217].

## 4. Large Synoptic Survey Telescope

The LSST is a powerful facility for cosmological studies. It will have an 8.4 m (6.5 m effective) primary mirror, a  $9.6 \text{ deg}^2$  FoV, and a 3.2 Gigapixel camera. An illustration of the LSST Observatory is shown in figure 3. This system will have unprecedented optical throughput and can image about  $10,000 \text{ deg}^2$  of sky in three clear nights using 30 s “visits” per each sky patch twice per night, with typical  $5\sigma$  depth for point sources of  $r \sim 24.5$  (AB magnitude). The detailed cadence will be decided by the Science Advisory Committee via simulations of observing scenarios. The system is designed to yield high image quality as well as superb astrometric and photometric accuracy. The project is in the construction phase and will begin regular survey operations by



**Figure 3.** The LSST Observatory: artist’s rendering of the dome enclosure with the attached summit support building on Cerro Pachón in Northern Chile. The LSST calibration telescope is shown on an adjacent rise to the right. Image credit: the LSST Project/NSF/AURA.

2022. The survey area will be imaged multiple times in six bands, *ugrizy*, covering the wavelength range 320–1050 nm. About 90% of the observing time will be devoted to a deep-wide-fast survey mode which will uniformly observe an  $18,000 \text{ deg}^2$  region of the southern sky over 800 times (summed over all six bands) during the anticipated 10 years of operations, and yield a co-added map to  $r \sim 27.5$ . These data will result in a relational database including 20 billion galaxies and a similar number of stars, and will serve the majority of the primary science programs. The remaining 10% of the observing time will be allocated to special projects such as a very deep and fast time domain survey. The goal is to make LSST data products including the relational database of about 30 trillion observations of 37 billion objects available to the public and scientists around the world.

#### 4.1. Telescope and camera

The large LSST étendue is achieved in a novel three-mirror design (modified Paul-Baker Mersenne-Schmidt system) with a very fast  $f/1.2$  beam [29]. The optical design has been optimized to yield a large FoV, with seeing-limited image quality, across a wide wavelength band. Incident light is collected by an annular primary mirror, having an outer diameter of 8.4 m and inner diameter of 5 m, creating an effective filled aperture of  $\sim 6.5$  m in diameter. The collected light is reflected to a 3.4 m convex secondary, then onto a 5 m concave tertiary, and finally into the three refractive lenses of the camera. In broad terms, the primary-secondary mirror pair acts as a beam condenser, while the aspheric portions of the secondary and tertiary mirror act as a Schmidt camera. The

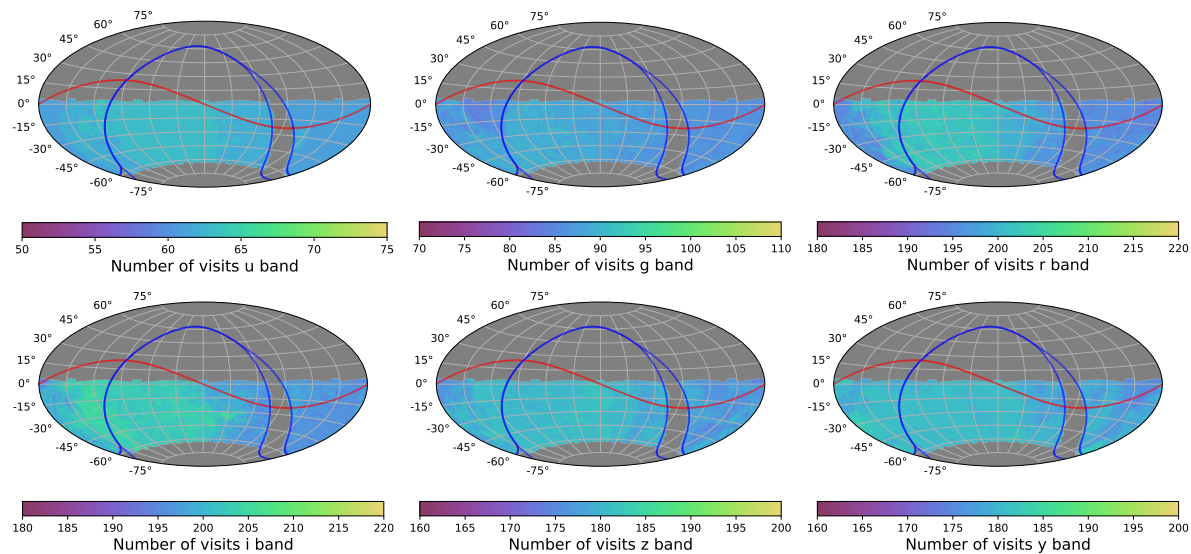


**Figure 4.** The distribution of the 6 band visits on the sky for a simulated realization of the baseline cadence. Image credit: Lynne Jones and the LSST Project/NSF/AURA.

3-element refractive optics of the camera correct for the chromatic aberrations induced by the necessity of a thick Dewar window and flatten the focal surface. All three mirrors will be actively supported to control wavefront distortions introduced by gravity and environmental stresses on the telescope.

The LSST camera provides a 3.2 Gigapixel flat focal plane array, tiled by 189  $4K \times 4K$  CCD sensors with  $10 \mu\text{m}$  pixels. This pixel count is a direct consequence of sampling the  $9.6 \text{ deg}^2$  FoV ( $0.64 \text{ m}$  diameter) with  $0.2 \text{ arcsec} \times 0.2 \text{ arcsec}$  pixels (Nyquist sampling in the best expected seeing of  $\sim 0.4 \text{ arcsec}$ ). The sensors are deep-depleted high-resistivity silicon back-illuminated devices with a highly segmented architecture that enables the entire array to be read in 2 seconds. The CCDs are grouped into  $3 \times 3$  rafts, each containing its own dedicated electronics. The rafts are mounted on a silicon carbide grid inside a vacuum cryostat, with an intricate thermal control system that maintains the CCDs at an operating temperature of 173 K. The entrance window to the cryostat is the third of the three refractive lenses in the camera. The other two lenses are mounted in an optics structure at the front of the camera body, which also contains a mechanical shutter, and a carousel assembly that holds five large optical filters. The sixth optical filter can replace any of the five via a procedure accomplished during daylight hours.

#### 4.2. Survey plan and performance

The main deep-wide-fast survey (typical single visit depth of  $r \sim 24.5$ ) will use about 90% of the observing time. The remaining 10% of the observing time will be used to obtain improved coverage of parameter space such as very deep observations. These deeper fields (deep-drilling fields) will aid in statistical completeness studies for the

**Table 1.** The LSST Baseline Design and Survey Parameters

Quantity	Baseline Design Specification
Optical Config.	3-mirror modified Paul-Baker
Mount Config.	Alt-azimuth
Final f-ratio, aperture	f/1.234, 8.4 m
FoV, étendue	9.6 deg <sup>2</sup> , 319 m <sup>2</sup> deg <sup>2</sup>
Plate Scale	50.9 μm/arcsec (0.2" pix)
Pixel count	3.2 Gigapix
Wavelength Coverage	320 – 1050 nm, <i>ugrizy</i>
Single visit depths, design <sup>a</sup>	23.9, 25.0, 24.7, 24.0, 23.3, 22.1
Mean number of visits <sup>b</sup>	56, 80, 184, 184, 160, 160
Final (coadded) depths <sup>c</sup>	26.1, 27.4, 27.5, 26.8, 26.1, 24.9

<sup>a</sup> Design specification from the Science Requirements Document (SRD) [220] for  $5\sigma$  depths for point sources in the *ugrizy* bands, respectively. The listed values are expressed on AB magnitude scale, and correspond to point sources and fiducial zenith observations (about 0.2 mag loss of depth is expected for realistic airmass distributions).

<sup>b</sup> An illustration of the distribution of the number of visits as a function of bandpass, taken from Table 24 in the SRD.

<sup>c</sup> Idealized depth of coadded images, based on design specification for  $5\sigma$  depth and the number of visits in the penultimate row (taken from Table 24 in the SRD).

main survey, since they will likely have deep spectroscopy as well as infrared coverage from other facilities. The observing strategy for the main survey will be optimized for homogeneity of depth and number of visits. In times of good seeing and at low airmass, preference will be given to *r*-band and *i*-band observations which are used in WL. The visits to each field will be widely distributed in position angle on the sky and rotation angle of the camera in order to minimize systematic effects on the point-spread function (PSF), which could introduce shear systematics in faint galaxies. Simulations of LSST operations use actual weather data from the Chilean site. The detailed cadence in time and space across the sky is being optimized with these simulations. We show one such simulation of the 6 band coverage in figure 4 [218, 219].

The universal cadence proposal excludes observations in a region of 1000 deg<sup>2</sup> around the Galactic Center, where the high stellar density leads to a confusion limit at much brighter magnitudes than those attained in the rest of the survey. The anticipated total number of visits for a ten-year LSST survey is about 2.8 million. The per-band allocation of these visits is shown in table 1. The adopted time allocation (see table 1) includes a slight preference for the *r* and *i* bands because of their dominant role in star/galaxy separation and WL measurements.

Precise determination of the PSF across each image, accurate photometric and astrometric calibration, and continuous monitoring of system performance and observing

conditions will be needed to reach the full potential of the LSST mission. The dark energy science requires accurate photometric redshifts, so the LSST photometry will be calibrated to unprecedented precision. Auxiliary instrumentation, including a 1.5 m calibration telescope, will provide the calibration parameters needed for image processing, to calibrate the instrumental response of the LSST hardware [221], and to measure the atmospheric optical depth as a function of wavelength along the LSST line of sight [222].

### 4.3. Data products

The rapid cadence and length of the LSST observing program will produce approximately 15 TB per night of raw imaging data. The large data volume, the time domain aspects, and the complexity of processing involved makes it impractical to rely on the end users for the data reduction. Instead, the data collected by the LSST system will be automatically reduced to scientifically useful catalogs and images. Over the ten years of LSST operations and 11 data releases, this processing will result in cumulative *processed* data of about 500 PB for imaging, and over 50 PB for the catalog databases. The final data release catalog database alone is expected to be approximately 15 PB in size.

Data collected by the LSST telescope and camera will be automatically processed to *data products* — catalogs, alerts, and reduced images. These products are designed to enable a large majority of LSST science cases, without the need to work directly with the raw pixels. We give a high-level overview of the LSST data products here; further details may be found in the LSST Data Products Definition Document [223], which is periodically updated. These data will be served via a relational database.

Two major categories of data products will be produced and delivered by the LSST: Level 1 and Level 2. Level 1 are time domain: data products which support the discovery, characterization, and rapid follow-up of time-dependent phenomena. Level 2 data products are most relevant to cosmology: they are designed to enable systematics- and flux-limited science, and will be made available in annual Data Releases. These will include the single-epoch images, deep coadds of the observed sky, catalogs of objects detected in the LSST data, catalogs of sources (the detections and measurements of objects on individual visits), and catalogs of “forced sources” — measurements of flux on individual visits at locations where objects were detected by the LSST or other surveys. LSST Level 2 processing will rely on multi-epoch model fitting, or *MultiFit*, to perform near-optimal characterization of object properties. Although the coadded images will be used to perform object *detection*, the *measurement* of their properties will be performed by simultaneously fitting (PSF-convolved) models to single-epoch observations. An extended source model — a constrained linear combination of two Sérsic profiles — and a point source model with proper motion — will generally be fitted to each detected object.

For the extended source model fits, the LSST will characterize and store the shape of

the associated likelihood surface (and the posterior) – not just the maximum likelihood values and covariances. The characterization will be done by sampling, with up to  $\sim 200$  (independent) likelihood samples retained for each object. For reasons of storage cost, these samples may be retained only for those bands of greatest interest for WL studies.

While a large majority of science cases will be adequately served by Level 1 and 2 data products, a limited number of highly specialized investigations may require custom, user-driven, processing of LSST data. This processing will be most efficiently performed at the LSST Archive Center, given the size of the LSST data set and the associated storage and computational challenges. To enable such use cases, the LSST DM system will devote the equivalent of 10% of its processing and storage capabilities to creation, use, and federation of so-called “Level 3” (user-created) data products. It will also allow the science teams to use the LSST database infrastructure to store and share their results. The LSST Archive Center and U.S. data access center will be at the National Center for Supercomputing Applications (NCSA) [224]. Users will access the LSST data through a Data Access Center web portal, a Jupyter Notebook interface, and machine accessible web application programming interfaces. The web portal will provide data access and visualization services, and the Notebook interface will enable more sophisticated data analysis.

#### *4.4. Engaging the community*

The LSST database and the associated object catalogs will be made available to the U.S. and Chilean scientific communities and to international partners with no proprietary period. The LSST project has been working with international partners to make LSST data products available worldwide. User-friendly tools for data access and exploration will be provided by the LSST data management system. This will support user-initiated queries and will run on LSST computers at the archive facility and the data access centers.

Because of the volume of the LSST data, statistical noise will reach unprecedented low levels so that some investigations will be limited by systematics, although at a level far below those of previous surveys. Thus, those investigations will require organized teams working together to optimize science analyses. LSST science collaborations have been established in core science areas. The LSST DESC includes members with interests in dark energy and related topics in fundamental physics.

The LSST Project is actively seeking and implementing input by the LSST science community. The LSST science collaborations in particular have helped develop the LSST science case and continue to provide advice on how to optimize their science with choices in cadence, software, and data systems. During the commissioning period, the Science Collaborations will play a role in the system optimization. The LSST Science Advisory Committee provides a formal dialogue with the science community. This committee also deals with technical topics of interest to both the science community and to the LSST Project, and shares responsibility for policy questions with the Project

Science Team.

## 5. LSST Probes of Cosmology

With its deep-wide-fast multiband imaging survey, the LSST will enable multiple probes simultaneously for cosmological studies. Here we discuss several probes that have been studied extensively: WL, LSS (or BAO<sup>¶</sup>), SNe Ia, galaxy clusters, and strong lensing. WL is considered the most powerful among these probes, and, at same time, it also imposes the most stringent requirements on the project (the telescope, data management, and operations) and beyond (e.g., analysis pipelines, computing infrastructure, simulations, theories, and so on). Since dark energy, or cosmic acceleration in general, has become a common science driver of almost every large extragalactic survey, these probes are often associated with dark energy, even though they are also sensitive to various elements of cosmology as can be inferred from section 3.

It is worth emphasizing the strength of utilizing multiple probes of the same survey as well as those of different surveys to address the fundamental questions about the universe. These probes will not only form interlocking cross-checks but also provide means of calibrating mutual systematics, which would be a common challenge for surveys like the LSST. The combination of WL and BAO is a particularly effective probe which breaks degeneracies and suppresses systematics.

We note that one probe can be analyzed using the methods of another probe. For example, in addition to their mass function, galaxy clusters may be studied for the LSS that they trace and their WL and strong lensing effects. Different statistics can also be applied to the same observables of each probe. For brevity, we introduce below only the most discussed method(s) and statistic(s) for each probe.

### 5.1. Large-scale structure (BAO)

Statistical analysis of the large-scale galaxy distribution is the main tool of LSS studies. Although LSS based on imaging data alone does not place strong constraints on the dark energy EoS, it is generally more sensitive than other LSST probes to cosmological parameters that affect the shape of the underlying matter power spectrum. LSS is a quite mature field with decades of studies (e.g., [44]), and its formulism can find applications in WL as well.

The LSST “gold sample” is expected to contain at least 2.6 billion galaxies at  $i_{AB} \leq 25.3$  mag. The redshift distribution is expected to follow  $n(z) \propto z^2 \exp(-3.2z)$  with an integrated surface number density of more than 40 arcmin<sup>-2</sup> [30, section 3.7]. Although it is advantageous to utilize the full posterior probability distribution of the

<sup>¶</sup> Much of the cosmological constraining power of the LSS in the LSST photo- $z$  galaxy sample is from the BAOs in the galaxy angular power spectra, so we use LSS and BAO interchangeably for the LSST unless it is necessary to make a distinction.

photometric redshift (photo- $z$ ) of each galaxy [225–227], we assume for convenience that a photo- $z$  is assigned to each galaxy. The science requirement on the photo- $z$  rms error per galaxy is  $\sigma_z(z) \leq \sigma_{z0}(1+z)$  with  $\sigma_{z0} = 0.05$ , and the goal is to achieve  $\sigma_z(z) \sim 0.02(1+z)$ . However, even with  $\sigma_{z0}$  as small as 0.02, the line-of-sight clustering information is still severely suppressed at  $k \gtrsim 0.02 h\text{Mpc}^{-1}$  [173, 228]. Therefore, it is more practical to focus on angular clustering of the galaxies between photo- $z$  bins.

With the Limber approximation [229], the galaxy angular power spectrum  $C_{ij}(\ell)$  is given by

$$C_{ij}(\ell) = \frac{2\pi^2}{c\ell^3} \int_0^\infty dz H(z) D_A(z) W_i(z) W_j(z) \Delta^2(k; z) + \delta_{ij}^K \frac{1}{\bar{n}_i} \quad (26)$$

$$W_i(z) = b(z) n_i(z) / \bar{n}_i, \quad (27)$$

where  $i$  and  $j$  identify the photo- $z$  bins,  $\ell$  is the multipole number,  $k = \ell/D_A$ ,  $\delta_{ij}^K$  is the Kronecker delta function,  $b(z)$  is the linear galaxy clustering bias,  $n_i(z)$  is the redshift distribution of galaxies in bin  $i$ , and  $\bar{n}_i = \int n_i(z) dz$ . The last term on the right-hand side of (26) is the shot noise due to discrete sampling of the continuous density field with galaxies. The covariance between the power spectra  $C_{ij}(\ell)$  and  $C_{mn}(\ell)$  per angular mode is given by

$$\text{Cov}[C_{ij}(\ell), C_{mn}(\ell)] = C_{im}(\ell) C_{jn}(\ell) + C_{in}(\ell) C_{jm}(\ell), \quad (28)$$

and the rms error of  $C_{ij}(\ell)$  is approximately

$$\sigma[C_{ij}(\ell)] = \left[ \frac{C_{ii}(\ell) C_{jj}(\ell) + C_{ij}^2(\ell)}{f_{\text{sky}}(2\ell + 1)} \right]^{1/2}, \quad (29)$$

where  $f_{\text{sky}}$  is the fraction of sky covered by the survey, e.g.,  $f_{\text{sky}} = 0.44$  for the LSST.

The scale dependence of the galaxy bias becomes more pronounced below tens of  $h^{-1}\text{Mpc}$ , so one has to limit the application of (26) to large scales, or model the bias in detail [63–65], or determine the galaxy bias with higher-order statistics [230, 231]. Equation (26) is also inaccurate on very large scales because the Limber approximation breaks down; if primordial non-Gaussianity is considered, the galaxy bias needs to be replaced by an effective bias that scales roughly as  $k^{-2}$  on very large scales [232, 233].

As an example, we show several galaxy angular power spectra in figure 5. The LSST gold sample is assigned to 30 bins from photo- $z$  of 0.15 to 3.5 with the bin width proportional to  $1+z$  in order to match the photo- $z$  rms error. Five auto power spectra in their respective bins are given in the left panel of figure 5. The power spectra are truncated at the high- $\ell$  end where nonlinear evolution starts to become important. Details of the calculations including the photo- $z$  treatment can be found in [174]. The right panel of figure 5 shows four cross power spectra between the bin centered on  $z = 1.66$  and its neighbors, and the auto spectrum at  $z = 1.66$  is included for reference. The amplitude of the cross power spectrum is largely determined by the overlap between the two bins in true redshift space, so it decreases rapidly with the bin separation under the Gaussian photo- $z$  model. This property can help calibrate the photo- $z$  error distribution [174, 234].

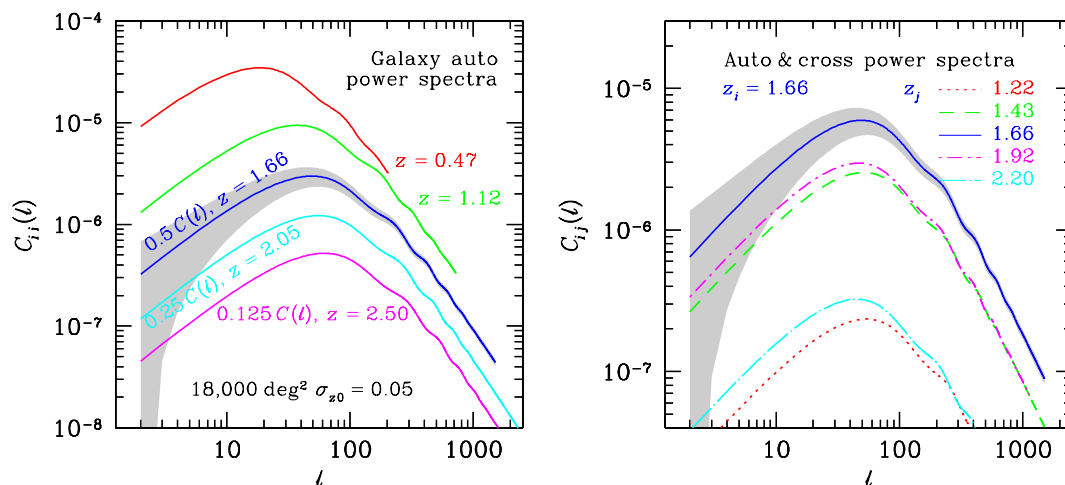


**Figure 5.** *Left panel:* Galaxy angular auto power spectra in five redshift bins (shifted for clarity). The central photo- $z$  of each bin is as labeled. The gray area indicates the statistical error (cosmic variance and shot noise) *per multipole* for the bin centered at  $z = 1.66$ . *Right panel:* Cross power spectra between bin  $i$  centered at  $z = 1.66$  and bin  $j$  centered at  $z = 1.22$  (4th neighbor, dotted line), 1.43 (2nd neighbor, dashed line), 1.92 (2nd neighbor, dash-dotted line), and 2.20 (4th neighbor, long-dash-dotted line). The auto power spectrum at  $z = 1.66$  is the same as that in the left panel. Figure adapted from [30] with updated survey data model.

One can clearly identify the BAO wiggles in the galaxy angular power spectra in figure 5 despite the projection of three-dimensional fluctuations onto the sphere. These wiggles are an imprint of acoustic waves in the tightly coupled cosmic fluid before the universe became sufficiently cool to form neutral hydrogen around  $z \simeq 1100$ . The primary CMB temperature anisotropy is a snapshot of these acoustic waves at the last scattering surface, which is characterized by the sound horizon  $r_s \sim 150$  Mpc at that time [176–178]. The BAO feature is mainly a function of the matter density and the baryon density, and its scale is large enough to remain nearly unchanged in comoving space since  $z \simeq 1100$ . Therefore, it can serve as a standard ruler to measure angular diameter distances (and Hubble parameters as well if accurate redshifts can be obtained) and to further constrain cosmological parameters [150–152, 235–237]. Recent spectroscopic BAO surveys have measured several distances up to  $z = 2.3$  with precision of a few percent [238–241]. The LSST gold sample will enable more distance measurements at the percent level up to  $z = 3$  with BAOs only [159].

It is recognized that nonlinear evolution modifies the BAO feature over time by damping its amplitude and shifting its scale by a fraction of a percent [242–245]. These effects can be calibrated with simulations. Figure 6 demonstrates the damping effect on the correlation functions at  $z = 0$ . The wiggles in the power spectrum become a peak in the correlation function near  $r_s \sim 110 h^{-1}$  Mpc. The BAO signal in the nonlinear dark matter correlation function (solid line, calculated with renormalized perturbation theory [246]) has less contrast than that in the linear dark matter correlation function (dotted line), and the shift of the BAO scale is not easily discernible. Although

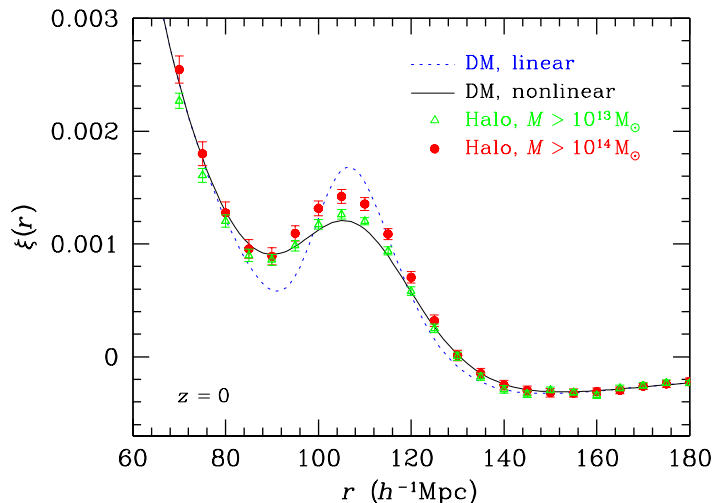


**Figure 6.** Damping of the BAO signal at  $z = 0$ . The dashed line and the solid line represent, respectively, the linear dark matter correlation function and the nonlinear dark matter correlation function. The correlation function of  $M > 10^{14} h^{-1} M_{\odot}$  halos from  $N$ -body simulations is plotted with filled circles, and that of  $M > 10^{13} h^{-1} M_{\odot}$  halos is plotted with open triangles. These correlation functions are normalized in the range of 160–180 Mpc. Data from [58].

not shown, the correlation function of dark matter particles in  $N$ -body simulations agrees well with the predicted nonlinear dark matter correlation function. The BAO signal of  $M > 10^{14} h^{-1} M_{\odot}$  halos (solid circles), however, experiences less damping. It is interesting to note that current galaxy BAO measurements all show stronger BAO signal than expected (e.g., [238–241]). Such an effect has little impact on cosmological constraints if one only uses the BAO scale information. However, a proper analysis utilizing the full correlation function(s) could gain significantly over *Planck* on parameters such as  $\omega_m$ ,  $\omega_b$ , and  $\Omega_k$  [174].

## 5.2. Weak gravitational lensing (WL)

Gravitational lensing is a ubiquitous phenomenon. In most cases, the distortion on background sources, e.g., galaxies, is so weak that it can only be detected statistically [247–249]. Since the lensing effect is caused by a foreground mass distribution, its statistics reflect those of the foreground and can be used to probe cosmology. In this subsection, we only consider two-point statistics of the shear and magnification effects of WL. Interested readers are referred to [250, 251] for a wealth of WL topics.

Given a lensed image in coordinates  $\boldsymbol{\theta}$ , one can recover the unlensed source in coordinates  $\boldsymbol{\beta}$  with the local distortion matrix

$$\mathbf{A} = \frac{\partial \boldsymbol{\beta}}{\partial \boldsymbol{\theta}} = \begin{pmatrix} 1 - \kappa - \gamma_1 & -\gamma_2 \\ -\gamma_2 & 1 - \kappa + \gamma_1 \end{pmatrix}, \quad (30)$$

where the convergence  $\kappa$  and shear components  $\gamma_i$  are related to the two-dimensional lensing potential  $\psi(\boldsymbol{\theta})$  via  $\kappa = \frac{1}{2} (\partial_{11}^2 \psi + \partial_{22}^2 \psi)$ ,  $\gamma_1 = \frac{1}{2} (\partial_{11}^2 \psi - \partial_{22}^2 \psi)$ , and  $\gamma_2 = \partial_{12}^2 \psi$ .

The convergence for a source at  $(\boldsymbol{\theta}, z)$  is a weighted integral of the overdensity along the line of sight

$$\kappa(\boldsymbol{\theta}, z) = \frac{3H_0^2\Omega_m}{2cD_A(z)} \int_0^z dz' \frac{D_A(z', z)D_A(z')}{H(z')} \delta(\boldsymbol{\theta}, z')(1+z'). \quad (31)$$

The lensing magnification is given by  $\mu = [(1 - \kappa)^2 - \gamma^2]^{-1}$ . In the WL regime,  $|\kappa|$  and  $|\gamma|$  are much smaller than unity, so that  $\mu \simeq 1 + 2\kappa$ . For convenience, we use the word ‘‘magnification’’ to also cover the case of demagnification.

Assuming that galaxies are randomly oriented in the absence of lensing, one can estimate the shear from the average galaxy ellipticities within an area of appropriate size. In practice, shear measurement is rather difficult, and it constitutes a major source of systematic errors for WL. Much effort is being made to improve the accuracy of shear measurement [e.g., 252–255]. Magnification changes the angular size of the background in different directions while conserving the  $4\pi$  solid angle as viewed by the (freefall) observer. To be specific, let  $\mu > 1$  in a particular direction. On the one hand, background galaxies are enlarged in this direction without altering their surface brightness, so they appear brighter in terms of total flux. Since the apparent magnitude is usually important for sample selection, faint galaxies that do not actually meet the magnitude criterion could make the cut with the slight lensing boost. This effect would increase the galaxy overdensity in the direction. On the other hand, magnification also increases the angular separation between the background galaxies, reducing their apparent surface density. These two competing effects do not cancel in general, and the resulting galaxy number density fluctuations of the sample is another useful probe of cosmology [256–259].

Angular power spectra (or two-point correlation functions) of shear signals are the primary statistics of WL. They can be written in a similar form as (26)

$$C_{ij}^{\gamma\gamma}(\ell) = \frac{2\pi^2}{c\ell^3} \int_0^\infty dz H(z)D_A(z)W_i^\gamma(z)W_j^\gamma(z)\Delta^2(k; z) + \delta_{ij}^K \frac{\sigma_\gamma^2}{\bar{n}_i}, \quad (32)$$

$$W_i^\gamma(z) = \frac{3\Omega_m H_0^2}{2} \frac{D_A(z)}{H(z)} \frac{1}{ac} \int_z^\infty dz' \frac{n_i(z')}{\bar{n}_i} \frac{D_A(z, z')}{D_A(z')}, \quad (33)$$

where  $\sigma_\gamma \sim 0.2$  is the rms shear of galaxies’ shape. The last term in (32) is known as the shape noise, analogous to the shot noise in galaxy power spectra. The window function  $W_i^\gamma(z)$  is a broad function in redshift, peaking roughly midway between the sources and the observer, so the cross power spectrum between two photo- $z$  bins has an amplitude close to that of the auto power spectrum in the lower photo- $z$  bin.

It is customary to decompose the effects of shear systematics on the power spectrum into multiplicative and additive components. The former arises from errors that are correlated with the true shear signal, whereas the latter is uncorrelated with the signal. The observed shear power spectra are then given by

$$\tilde{C}_{ij}^{\gamma\gamma}(\ell) = (1 + f_i)(1 + f_j)C_{ij}^{\gamma\gamma}(\ell) + C_{ij}^{\text{add}}(\ell), \quad (34)$$

where  $f_i$  and  $f_j$  account for the multiplicative errors, and  $C_{ij}^{\text{add}}(\ell)$  is the power spectrum of the additive errors. In principle, these forms of errors also exist in the galaxy power

spectra, but results from existing galaxy surveys suggest that they are sub-dominant. For the LSST, the multiplicative errors of the shear power spectra need to be controlled below 0.004 [260, 261], which is challenging. The dominant issue for ground-based imaging is the PSF correction and its misestimation. This is particularly important for tomographic cosmic shear where the evolution of the multiplicative correction to the observed shear must correctly track the evolving size distribution of the source galaxies with redshift. This low level of correction can be achieved for a deep tomographic WL cosmic shear survey via simulations of the observations [262, 263]. For additive shear it is not trivial to accurately determine the scale dependence of  $C_{ij}^{\text{add}}(\ell)$ , but the level of additive errors estimated from image simulations [264] suggests that it would not be overly important for the LSST [265]. There are also small additive and multiplicative PSF errors introduced by charge transport anomalies in the detector, however these can be well calibrated and removed to first order in pixel processing. These errors, particularly the multiplicative systematic, can be suppressed via observing strategy. The amplitudes of these errors decrease rapidly in good image quality: this translates to low airmass observing and a strategy of reimaging areas with previous poor seeing exposures. Special dithering of exposures in subsequent re-visits to a field, in position and camera angle, are planned.

The fact that WL measures directly the gravitational effect of all the matter and that it is sensitive to both the expansion of the universe and the growth of cosmic structures make it a powerful probe for the LSST, though it also has a number of challenges besides shear estimation. A major source of error is uncertainties in the photo- $z$  error distribution or, equivalently, those in the true redshift distribution of galaxies in each photo- $z$  bin. Because the lensing kernel is very broad, a small error in  $n_i$ , e.g., a shift of its central redshift by  $\Delta z \sim 0.01$ , has practically no effect on the shear power spectra. However, the cosmological interpretation would be sufficiently different even with such a small redshift error that dark energy constraints would be degraded considerably. It is recognized that the uncertainties in the mean and the width of the true-redshift distribution of galaxies in each photo- $z$  bin should not exceed a few  $10^{-3}(1+z)$  for the LSST [174, 260, 266]. To achieve this goal, calibrations of both individual galaxy redshift [267, 268] and the overall redshift distribution of the galaxies in each photo- $z$  bin are needed. The latter can be done to the required precision with correlations between spatially overlapping photo- $z$  and spectroscopic samples of brighter galaxies over small patches of the survey area [269, 270]. Correlations between different photo- $z$  bins arising from incorrect assignment of the galaxies will also be helpful for the calibration [174, 234, 271].

At the surface density of galaxies in the LSST gold sample, a small percentage will be partially blended with other galaxies in the sample. This can cause outliers in photo- $z$  and generate about a 7% increase in WL shear noise unless addressed at the galaxy level and statistically [272, 273]. If blends can be tagged (for example via a color gradient in the combined core) then they may be eliminated from the sample. Conspicuous blends with larger separation may be more easily identified, tagged and deblended.

Another challenge for WL is intrinsic alignment [274, 275]. The orientation of a galaxy can be influenced by the larger structure containing it, thus breaking the assumption that galaxies orient randomly in the absence of lensing. The correlation of galaxy orientations in the same structure would contaminate the true shear signal arising from these galaxies' common foreground mass distribution. Moreover, if these galaxies themselves are taken as the foreground, then the structure they reside in would lens galaxies in the background. The two effects of the same structure, intrinsic alignment of the foreground galaxies and shear on the background galaxies, would correlate the background and foreground galaxy orientations, contaminating the true correlation between these galaxies' shear signals. One needs to utilize photo- $z$  information and model the intrinsic alignment effects to minimize the impact on cosmology [276–279]. It is encouraging that marginalization of the intrinsic alignment systematics using a simple phenomenological model may be sufficient for shear analyses [280, 281]. For the LSST, faint blue galaxies will dominate its gold sample, and these are expected to be less affected by intrinsic alignment [282].

Since magnification is extracted from the observed galaxy density fluctuations, it avoids some of the difficulties with shear measurements but unfortunately inherits its own systematics. The galaxy overdensity with magnification effect is approximately [256, 283]

$$\delta^{\tilde{g}} \simeq b\delta + 5(s - 0.4)\kappa, \quad (35)$$

where  $s = d \log N/dm \sim 0.2\text{--}0.6$  is the logarithmic slope of the galaxy number counts at the limiting magnitude  $m$  of the sample [e.g., 284]. The total angular power spectrum of galaxies in photo- $z$  bins  $i$  and  $j$  becomes [285]

$$C_{ij}^{\tilde{g}\tilde{g}} = C_{ij}^{gg} + q_i C_{ij}^{\kappa g} + q_j C_{ij}^{g\kappa} + q_i q_j C_{ij}^{\kappa\kappa}, \quad (36)$$

where  $C_{ij}^{gg}$  is the power spectrum due to galaxy intrinsic clustering, i.e., (26) with the superscript  $g$  written out explicitly,  $q_i = 5(s_i - 0.4)$  with  $s_i$  for bin  $i$ ,  $q_i C_{ij}^{\kappa g}$  and  $q_j C_{ij}^{g\kappa}$  are the galaxy-magnification cross power spectra, and  $q_i q_j C_{ij}^{\kappa\kappa}$  is the magnification power spectrum. Since the convergence for a lower redshift bin is uncorrelated with the galaxy overdensity in a higher redshift bin, one of the cross terms vanishes for two well separated bins. The galaxy-convergence power spectra  $C_{ij}^{\kappa g}$  and  $C_{ij}^{g\kappa}$  and the convergence power spectrum  $C_{ij}^{\kappa\kappa}$  can be calculated using (32) but with the two shear window functions replaced by the galaxy window function (27) and the convergence window function, which is identical to the shear window function (33).

The intrinsic clustering term is several orders of magnitude greater than the rest in (36) when the photo- $z$  bins  $i$  and  $j$  overlap significantly in true-redshift space; even if they are well separated, the cross term  $C_{ij}^{g\kappa}$  — assuming that bin  $j$  is at higher redshift — still overwhelms  $C_{ij}^{\kappa\kappa}$  [286]. Furthermore, galaxies can be assigned to wrong redshift bins because of photo- $z$  errors, and the resulting spurious correlations can be a serious contaminant for the magnification signal (conversely, magnification in tomographic galaxy cross-correlations may be a contaminant for photo- $z$  self-calibration with the cross-correlations). Magnification systematic error can also arise from exposure

depth spatial variations, dust, and blending of galaxy images [287]. Therefore, like the case with shear, care must be taken when utilizing lensing magnification for precision cosmology. As a cosmological constraint, magnification is subdominant to the other WL probes.

### 5.3. Type Ia supernovae

SN Ia distances provided the most direct evidence for the accelerated cosmic expansion [14, 15] and will remain an important dark energy probe in the future, though systematic errors make it a less precise probe of cosmology by comparison to a joint analysis of WL and BAO. The LSST is expected to obtain more than ten thousand well observed SNe Ia ( $0.1 < z < 1.2$ ) in the deep-drilling fields, hundreds of thousands reasonably-well observed SNe Ia ( $z \lesssim 0.8$ ) in the main survey, and millions of detection-only SNe Ia [30]. Such a huge sample of SNe Ia will enable new tests of cosmology such as the isotropy of distance-redshift relation over the whole survey area.

The utility of SNe Ia for cosmology is based on their standardizable peak luminosity that is tightly correlated with the initial decline rate of the light curve [288]. As such, one can obtain the distance modulus, which is a function of cosmological parameters, via [289–291]

$$\mu_B = m_B - M_B + \alpha x_1 - \beta \mathcal{C} \quad (37)$$

where  $m_B$  is the rest-frame  $B$ -band peak apparent magnitude,  $M_B$  is the corresponding absolute magnitude,  $x_1$  is the shape parameter of the light curve,  $\mathcal{C}$  is the  $B - V$  color, and  $\alpha$  and  $\beta$  are nuisance parameters to be fitted along with  $M_B$  (actually  $M_B - 5 \log h$ ) and the cosmological parameters. Given the fairly low intrinsic dispersion of  $\mu_B$  of roughly 0.12, a single SN Ia can provide a luminosity distance with a nominal error of 6% (excluding the error in  $h$ ). It is worth mentioning that SNe Ia are likely to be more standard in the rest-frame near infrared [292, 293], though the LSST can observe only up to  $1.05 \mu\text{m}$ .

The degeneracy between the Hubble constant and  $M_B$  removes the absolute scale of SN Ia distances and thus weakens their constraints on the cosmological parameters. The remedy is to obtain a sample spanning as wide a redshift range as possible and to combine a tight prior on the Hubble constant from external datasets. A number of technical issues and systematic uncertainties could be the limiting factors for SN Ia cosmology with next-generation surveys. Besides the challenges of obtaining very well sampled light curves and precisely calibrated photometries, one also needs further investigation on potential evolution of SN Ia properties over redshift, the relation between the SN Ia peak luminosity and its host properties, and certainly the physics of SN Ia explosions.

The LSST survey, especially its deep-drilling fields, is tasked to address the technical challenges for SN Ia cosmology, though effort is still being made to optimize the operation strategy of the main survey. The huge LSST SN Ia sample can be divided into many sub-samples for detailed studies of various systematics intrinsic to SNe Ia themselves as well as biases arising from sample selection. Nonetheless, being an imaging

survey, the LSST has its own challenges. For example, it has to correctly identify SNe Ia and determine their redshifts based on photometric data only [294, 295]; even though a small fraction of them will have spectroscopic follow-ups by other facilities, the LSST still has to send out alerts promptly for the best candidates among millions of transients every night with very high success-rate. It is also noted that photo- $z$  errors increase the apparent dispersion of the standardized SN Ia peak luminosity and that the sample-averaged distance modulus–photo- $z$  relation departs from the distance modulus–true redshift relation [296]. One should account for these effects when estimating the cosmological parameters.

#### 5.4. Galaxy clusters

Galaxy clusters are the largest gravitationally bound systems in the universe. At the high-mass end, a cluster may have thousands of member galaxies, while a low-mass cluster can still contain many dozens of galaxies. Cluster cosmology is a rich topic and involves observations from microwave to X-ray [for a review, see 297]. The primary statistic of cluster cosmology for the LSST is the mass function, i.e., number density of clusters as a function of mass at a certain redshift. Since clusters have grown under gravitational instability from relatively high density regions of the fairly Gaussian initial density fluctuations, one can roughly estimate the cluster mass function based on the statistics of the Gaussian random field [298, 299]. For precision cosmology, more accurate mass functions need to be extracted from  $N$ -body simulations [300, 301].

The cluster mass function is sensitive to both the geometry of the universe and the growth of the large-scale structures, which makes it a powerful tool [302–304]. However, the utility of clusters for precision cosmology critically depends on the knowledge of the mass-observable relation and its scatter [305]. Because of the highly nonlinear process of cluster formation and evolution, one has to rely on state-of-the-art simulations and observations to precisely calibrate the mass-observable relation and its scatter for a wide range of cosmology. It takes considerably more effort to properly include all the relevant physics such as star formation and feedback in the simulations to reproduce the observables [e.g., 306–308].

The LSST will produce a well observed sample of several hundred thousand clusters, much larger than any previous surveys. It is not trivial to construct such a sample efficiently from the LSST photometry data with high purity, high completeness, and well understood selection function. Accurate photo- $z$ s are needed for clusters as well. Averaging over member galaxies’ redshifts generally reduces the photo- $z$  errors, but one has to be careful about any systematic redshift errors of the galaxy population in the same cluster. Although WL measurements from the same LSST data can provide important absolute cluster mass calibration, the scatter will be rather high ( $\gtrsim 20\%$ ), mainly due to triaxiality of the halos, projection effects along the line-of-sight, and shape noise of shear measurements in the limited FoV [309]. It has been shown for Dark Energy Survey (DES) that even a small fraction of the whole cluster sample (e.g., 200

out of  $10^5$  expected) calibrated against a mass proxy of 10% scatter can enhance the DES dark energy constraints by 50% [310]. As such, it is crucial to establish a tight relation between cluster observables from LSST data with the cluster mass through external low-scatter mass proxies, likely from X-ray observations [311].

### 5.5. Strong lensing

While WL effects are hardly discernible to the eye, background objects can be stretched into arcs or even Einstein rings and be split into multiple images in the strong lensing regime [e.g., 312–314]. A lens can be a galaxy or a galaxy cluster, and the background sources are usually galaxies that are effectively static within the time span of an observational program. In rare cases, one can find multiple-image systems of variable or transient background sources such as active galactic nuclei (AGNs) and SNe [315, 316]. Different images of the same source means different paths and travel times for the photons. The detailed configuration of the images and time delay between them are determined by the mass distribution of the lens and the angular diameter distances between the observer, the lens, and the source. Therefore, the strong-lensing time delay can be a useful probe of cosmology. It is most sensitive to the Hubble constant [317] and has recently been demonstrated to be able to constrain other cosmological parameters such as the curvature parameter  $\Omega_k$  and the dark energy EoS parameter  $w$  [318, 319].

The typical time delay of a double lens (double-image system) is 1-3 months, and much shorter delays of less than a day can occur when two images in a quad lens (quadruple-image system) are very close to each other [320]. The LSST’s 10-year rolling survey with 3-month seasons and a cadence of 5 days is suited for time delay measurements of typical strong lensing systems. It is estimated that the LSST strong lens sample will be at least an order of magnitude larger than previously obtained, allowing time delays to be measured for more than 3000 strongly lensed quasars and more than 100 strongly lensed SNe [320].

Like other LSST probes, strong-lensing time delay has its own challenges. Besides lens monitoring and fitting for the time delay, one would also need accurate information about the lens mass distribution and the source redshift. Moreover, the impact of line-of-sight mass distribution on time delay needs to be taken into account, at least statistically. In these areas, high-resolution observations from space, deep spectroscopy on the ground, and modeling of the foreground structures will be particularly helpful for strong-lensing cosmology with the LSST. In fact, with a major undertaking of external follow-up observations, one can also probe the geometry of the universe with strongly lensed sources in multiple source planes [321–323].

### 5.6. Joint analyses

The ability to produce large uniform data sets with high quality for multiple cosmological probes is a crucial advantage of the LSST. These probes are affected by various systematics and are sensitive to cosmology in different ways. Joint analyses of multiple

probes not only improve parameter constraints but, more importantly, also enable certain cross-calibrations of known systematics and detection of unknown systematics. This allows one to perform robust tests on cosmological models and to explore with confidence fundamental physics of the universe beyond current understanding.

The aforementioned probes are not always statistically independent. Correlations arise when two probes are linked by common factors of real physical origin or observational effects. For instance, WL shear of background galaxies is essentially a function of the weighted projection of the line-of-sight mass distribution, which is traced by galaxies. Thus, foreground galaxy density fluctuations are correlated with the background shear, similar to the case of lensing magnification in section 5.2. This effect is known as the galaxy-shear correlation or galaxy-galaxy lensing on large scales ( $\ell \lesssim 1000$ ) [63, 174, 324, 325], though, strictly speaking, the former can also include a contribution from intrinsic alignment. The fact that WL and LSS (or BAO) techniques share, at least partially, the same catalog of galaxies, and their photo- $z$  systematics also induces a correlation between the two probes. Such a correlation can be beneficial, as the self-calibration of the photo- $z$  error distribution by cross-bin galaxy power spectra can reduce the sensitivity of the joint cosmological constraints of WL and BAO to uncertainties in the photo- $z$  error distribution [174, 234, 271]. Conversely, because of the shared dark matter structure, the complementary WL and BAO measurements break degeneracies in either probe.

Figure 7 demonstrates the synergy between WL and BAO based on Fisher matrix analyses [67, 327, 328]. It is adapted from [326] with the survey area, galaxy redshift distribution, and galaxy surface number density, respectively, adjusted to  $18,000 \text{ deg}^2$ ,  $n(z) \sim z^2 \exp(-z/0.3)$ , and  $40 \text{ arcmin}^{-2}$ . The number density is an effective value for WL measurements, and the same is applied to BAO for convenience. The constraints of the joint analysis are derived from the full set of galaxy-galaxy (i.e., galaxy clustering), galaxy-shear (i.e., galaxy-galaxy lensing), and shear-shear power spectra. These power spectra are affected by different powers of the galaxy bias and together can achieve robust cosmological constraints in the presence of uncertainties in the galaxy bias [63, 174]. Numerically, the galaxy-shear power spectra are equal to the galaxy-convergence power spectra  $C_{ij}^{g\kappa}$  in section 5.2. *Planck* CMB priors from a Fisher matrix calculation in [174] are applied to all the results. While the constraints on the dark energy EoS parameters,  $w_0$  and  $w_a$ , from shear power spectra alone are sensitive to systematic uncertainties in the photo- $z$  error distribution, the joint results of shear and galaxy power spectra remain fairly immune to these systematics. The dramatic improvement of the joint results over the WL-only results is due to the mutual calibration of the photo- $z$  uncertainties as well as the uncertain factor of the galaxy bias. In other words, much of the complementarity is in parameter space that has been marginalized over. A demonstration of the constraining power of this joint analysis of cosmic shear, galaxy-galaxy lensing and angular clustering has recently been obtained [329].

A forecast of cosmological constraints from combinations of three LSST probes and real *Planck* data is given in figure 8. The *Planck* data consists of the joint likelihood of

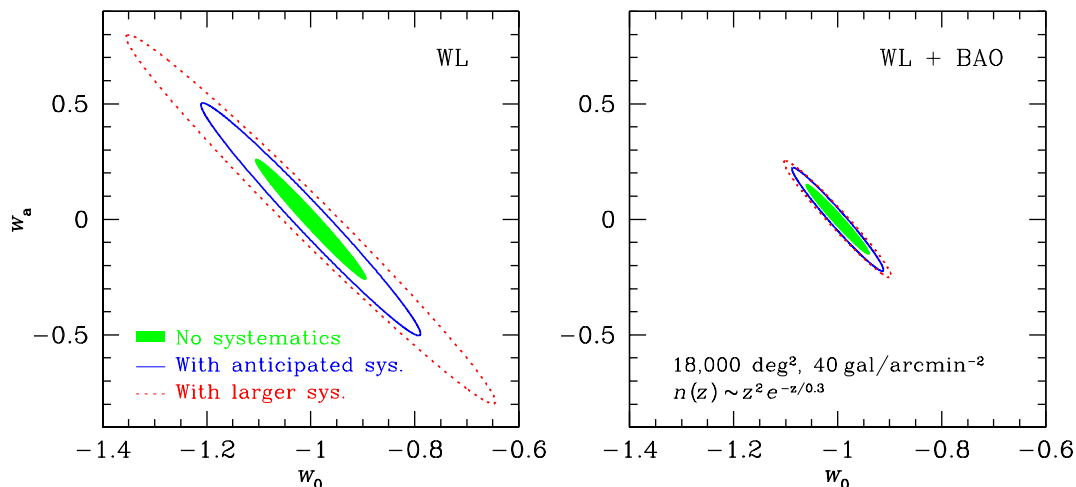


**Figure 7.** One-sigma error contours of the dark energy EoS parameters  $w_0$  and  $w_a$  from LSST WL shear power spectra alone (left panel) and shear and galaxy power spectra analyzed jointly (right panel). The shaded areas represent the results with statistical errors only. The solid contours correspond to those with the anticipated level of systematic errors, which include the uncertainty in the photo- $z$  error distribution and additive and multiplicative errors in the power spectra. The assumed photo- $z$  systematics would require a redshift calibration sample of 3000 spectra per unit redshift interval if the photo- $z$  error distribution were Gaussian. This calibration can be achieved statistically by using spectra of the brighter galaxies in the redshift interval in small areas of the sky. The dotted contours relax the requirement to 188 spectra per unit redshift. Figure adapted from [326] with updated survey data model.

the temperature-temperature (TT), temperature-E polarization (TE), E polarization-E polarization (EE), and B polarization-B polarization power spectra in the range of  $2 \leq \ell \leq 29$  and the foreground-marginalized joint likelihood of TT ( $30 \leq \ell \leq 2508$ ), TE ( $30 \leq \ell \leq 1996$ ), and EE ( $30 \leq \ell \leq 1996$ ) band power spectra [330]. The CMB power spectra are calculated using CLASS with the lensing effect turned on [175]. The LSST probes considered are WL, BAO, and SNe Ia. The set of cosmological parameters includes  $w_0$ ,  $w_a$ ,  $\omega_m$ ,  $\omega_b$ ,  $\Omega_k$ ,  $n_s$ ,  $H_0$ , the redshift of reionization  $z_{\text{rei}}$ , the helium fraction  $Y_p$ , and the amplitude of the curvature power spectrum  $A_s$ . The sum of neutrino masses is fixed at 0.06 eV.

The posterior probability distribution of the parameters are mapped with an affine invariant Markov Chain Monte Carlo sampler [331, 332]. For LSST WL and BAO, we use the corresponding Fisher matrices to calculate contributions to the final likelihood. The Fisher matrices have been marginalized over non-cosmological parameters such as those modeling the photo- $z$  errors, galaxy biases, and errors in the power spectra. The fiducial model of the Fisher matrices coincides with the *Planck*-only best-fit  $\Lambda$ CDM model [149], and the fiducial values of the additional parameters,  $w_0$ ,  $w_a$ , and  $\Omega_k$ , are set to  $-1$ ,  $0$ , and  $0$ , respectively. For LSST SNe Ia, a simple mock sample (tuples of distance modulus and redshift) is generated under the fiducial cosmological model according to the yields and redshift distributions from section 11.2 of [30]. The selection criterion is that each

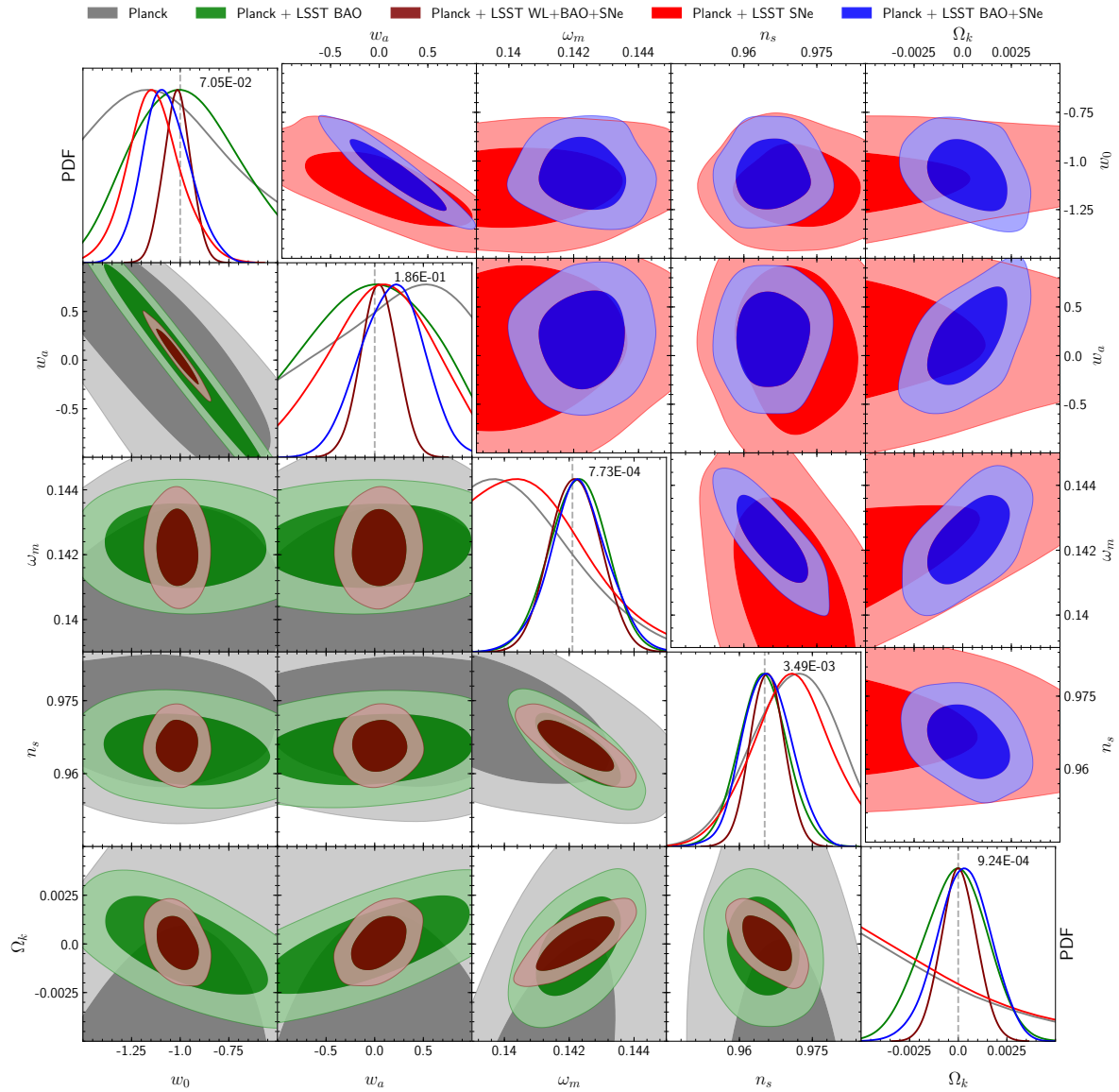


**Figure 8.** Forecast of cosmological constraints from combinations of three LSST probes and real *Planck* data. For a proper layout, only 5 parameters that benefit most from the LSST data are plotted. The probes are color-coded: *Planck*-only in gray, LSST SNe Ia plus *Planck* in red, LSST BAO plus *Planck* in green, LSST BAO+SNe Ia plus *Planck* in blue, and LSST WL+BAO+SNe Ia plus *Planck* in brown. The shades of the same color in each two-parameter panel fill the contours of 68% and 95% confidence level, respectively. The panels along the diagonal present the marginalized probability distribution functions of each parameter, which are normalized to have a maximum value of unity. The vertical dashed lines in the panels along the diagonal mark the parameters’ fiducial values, and the 1- $\sigma$  errors of LSST WL+BAO+SNe Ia plus *Planck* are also given in these panels.

SN must be observed in three or more filters at a minimum signal-to-noise ratio of 20, which results in roughly 400,000 SNe from the main survey and 12,000 SNe from the deep-drilling survey in 10 years. While the deep-drilling survey can be optimized for SN observations, it is impossible for the main survey to mass-produce SN light curves with the same quality as can be achieved by the former. To be conservative, we reduce the number of SNe Ia in the main sample somewhat arbitrarily to 100,000. The intrinsic dispersion of the standardized SN Ia peak absolute magnitude is assumed to be 0.13, and we adopt a photo- $z$  rms error model of  $\sigma_z = 0.02(1+z)$  [333–335]. Photo- $z$  bias errors and correlations between different SNe are neglected for simplicity. The likelihood of the SNe Ia is then evaluated in the conventional way [see, e.g., 336] with modifications to the fiducial distance modulus-redshift relation and apparent dispersion of the distance modulus to account for the effects of the photo- $z$  errors [296].

Figure 8 shows that the LSST is indeed more than a dark energy experiment. With the huge number of modes contained in the survey volume [173], LSST BAO is able to achieve significant enhancement over *Planck* on parameters that affect the shape of the matter power spectrum. The CMB can only determine one distance — the distance to the last scattering surface, so that *Planck* alone, even with the CMB lensing effect, does not provide useful constraints on  $w_0$ ,  $w_a$ , and  $\Omega_k$ . Moreover, the curvature parameter is pulled slightly negative:  $\Omega_k = -0.018^{+0.014}_{-0.009}$ . Similar behavior is observed by the *Planck* Collaboration as well when the  $\Lambda$ CDM model is extended to include  $\Omega_k$  [149]. The addition of LSST SNe Ia to *Planck* is particularly helpful on  $w_0$  and, to a lesser degree,  $w_a$ , but, as expected, not much is gained on the other parameters. The joint analysis of LSST WL+BAO+SNe Ia plus *Planck* places tight constraints on the dark energy EoS parameters, obtaining  $\sigma(w_0) = 0.07$ ,  $\sigma(w_a) = 0.19$ , and the minimum error of the EoS  $\sigma(w) = 0.017$  at the pivot redshift  $z = 0.58$ , and reduces the uncertainties on the other parameters moderately over those of LSST BAO plus *Planck*. Although not shown in figure 8, the joint results of LSST WL+BAO plus *Planck* are nearly identical to the all-probes results except that the errors on  $w_0$  and  $w_a$  are roughly 10% larger.

Since we have not included all the LSST cosmological probes in the forecast, there is still room for improvement on the constraints. Efforts are being made by the LSST DESC to develop a suite of software packages for comprehensive analyses of the data [33, 281]. Moreover, the  $w_0$ - $w_a$  parametrization does not capture the full complexity of all dark energy models and significantly underestimates the capabilities of Stage IV surveys like the LSST [133, 134]. It has been demonstrated that multiple dark energy EoS eigenmodes in redshift (or expansion factor) space can be reconstructed from the data with sufficiently small errors to allow tests of a wide variety of dark energy models [e.g., 337]. Finally, anisotropy in dark energy introduced, for example, by dark energy clustering can be detected in the LSST survey via two complementary methods [30, section 15.5].

## 6. Summary

The LSST holds great promise for breakthrough discoveries in cosmology, and, not surprisingly, it comes with challenges. While the LSST project works on the technological and engineering front, scientists have much to prepare for. On the one hand, the LSST survey will bring unprecedented statistical precision enabling knowledge beyond our current horizon, requiring extraordinary effort and often novel use of the data. On the other hand, like other large-scale surveys in the 2020s, the LSST is likely to remain limited by systematic errors arising from instruments, observations, data reduction, analysis methods, and even deficiencies in theories. We have largely skated over these important issues to avoid distraction by the details. Efforts on detecting and controlling systematics, especially those not yet known, are crucial for the LSST to reach for its full potential. In fact, a large fraction of the activities of the LSST DESC is devoted to systematics.

Much of the science produced by the LSST survey would greatly benefit from other data at a variety of wavelengths, resolutions, depths, and timescales. The *Euclid* mission [338] and the Wide Field Infrared Survey Telescope (*WFIRST*) [339] can provide near-infrared photometry data in the area partially overlapping with the LSST survey. The galaxy spectral energy distributions derived from the combined data should give rise to even better photometric redshifts as well as tighter constraints on stellar masses and star formation histories crucial for galaxy evolution studies. The WL analyses from space and from the ground will be highly complementary and will provide cross-checks of one another. More importantly, in a subset of the survey area, *Euclid* and *WFIRST* spectra of galaxies in the bright part of the LSST photometric sample will efficiently calibrate the LSST photo- $z$  error distributions in redshift bins.

The LSST will also enable multi-wavelength studies of faint optical sources using gamma-ray, X-ray, infrared and radio data. The LSST will provide a crucial complementary capability to space experiments operating in other wavebands, such as the ongoing Nuclear Spectroscopic Telescope Array [340] and the *Fermi* Gamma-ray Space Telescope [e.g., 341]. The large samples of various astronomical source populations will yield both representative objects of each population with exquisite statistics and extremely rare objects for investigations by powerful facilities such as the James Webb Space Telescope [342] and the next generation of 30–40 m telescopes [343–345]. Better understanding of these sources, especially on the subject of galaxy evolution, will in turn aid the cosmological data analysis. The Square Kilometer Array [346] will extend the cross calibration using a large sample of galaxies in the radio.

There is no doubt that close collaborations between the LSST and its peers will make “the whole greater than the sum of the parts” [347]. However, with other surveys, the full benefit is likely to require joint reduction and analyses of the data at fairly low levels, e.g., images as opposed to catalogs; in other cases, concerted observational campaigns of serious undertaking may be necessary.

The LSST will be transformative in many areas beyond astronomy and physics as

sciences and beyond astronomy and physics as communities. The most exciting aspect of the LSST is the enormous discovery space it offers. What we have imagined of the LSST today may well be only the tip of the iceberg when the survey unfolds.

## Acknowledgments

Financial support for the LSST comes from the NSF through Cooperative Agreement No. 1258333, the Department of Energy Office of Science under Contract No. DE-AC02-76SF00515, and private funding raised by the LSST Corporation. HZ was partially supported by the National key Research Program of China grant No. 2016YFB1000605. We thank Youhua Xu for assistance in producing the figures, and Michael Schneider, Seth Digel, Zeljko Ivezic and the anonymous referee for helpful suggestions for the manuscript.

## References

- [1] Hubble E P 1936 *Realm of the Nebulae* (Yale University Press) ISBN 9780300025002
- [2] Penzias A A and Wilson R W 1965 A Measurement of Excess Antenna Temperature at 4080 Mc/s. *Astrophys. J.* **142** 419–421
- [3] Science Advisory Structure of ESA 2005 *Cosmic Vision: Space Science for Europe 2015-2025* ISBN 9290924896 URL <http://sci.esa.int/CVplan>
- [4] National Research Council 2010 *New Worlds, New Horizons in Astronomy and Astrophysics* (Washington DC: National Academies Press) ISBN 9780309157995 URL <https://doi.org/10.17226/12951>
- [5] National Research Council 2003 *Connecting Quarks with the Cosmos: Eleven Science Questions for the New Century* (Washington DC: National Academies Press) ISBN 9780309074063 URL <https://doi.org/10.17226/10079>
- [6] High Energy Physics Advisory Panel, DOE/NSF 2004 *Quantum Universe: the Revolution in 21st Century Particle Physics* URL <https://science.energy.gov/hep/hepap/reports/>
- [7] Tyson J A, Valdes F, Jarvis J F and Mills Jr A P 1984 Galaxy mass distribution from gravitational light deflection *Astrophys. J. Lett.* **281** L59–L62
- [8] Schneider D P, Turner E L, Gunn J E, Hewitt J N, Schmidt M and Lawrence C R 1988 High-resolution CCD imaging and derived gravitational lens models of 2237+0305 *Astron. J.* **95** 1619–1628
- [9] Tyson J A, Valdes F and Wenk R A 1990 Detection of systematic gravitational lens galaxy image alignments - Mapping dark matter in galaxy clusters *Astrophys. J. Lett.* **349** L1–L4
- [10] Kneib J P, Mellier Y, Fort B and Mathez G 1993 The Distribution of Dark Matter in Distant Cluster Lenses - Modelling A:370 *Astron. & Astrophys.* **273** 367
- [11] Fahlman G, Kaiser N, Squires G and Woods D 1994 Dark matter in MS 1224 from distortion of background galaxies *Astrophys. J.* **437** 56–62 (*Preprint astro-ph/9402017*)

- [12] Tyson J A, Bernstein G M, Blouke M M and Lee R W 1992 Large-area CCD mosaic for astronomical imaging *High-Resolution Sensors and Hybrid Systems (Proc. SPIE vol 1656)* pp 400–408 URL <http://dx.doi.org/10.1117/12.135921>
- [13] Wittman D M, Tyson J A, Bernstein G M, Lee R W, dell’Antonio I P, Fischer P, Smith D R and Blouke M M 1998 Big Throughput Camera: the First Year *Optical Astronomical Instrumentation (Proc. SPIE vol 3355)* ed D’Odorico S pp 626–634
- [14] Riess A G et al 1998 Observational Evidence from Supernovae for an Accelerating Universe and a Cosmological Constant *Astron. J.* **116** 1009–1038 (*Preprint astro-ph/9805201*)
- [15] Perlmutter S et al and The Supernova Cosmology Project 1999 Measurements of Omega and Lambda from 42 High-Redshift Supernovae *Astrophys. J.* **517** 565–586 (*Preprint astro-ph/9812133*)
- [16] York D G et al and SDSS Collaboration 2000 The Sloan Digital Sky Survey: Technical Summary *Astron. J.* **120** 1579–1587 (*Preprint astro-ph/0006396*)
- [17] Adelman-McCarthy J K et al 2007 The Fifth Data Release of the Sloan Digital Sky Survey *Astrophys. J. Supp.* **172** 634–644 (*Preprint 0707.3380*)
- [18] URL <http://dls.physics.ucdavis.edu/>
- [19] URL <http://www.cfht.hawaii.edu/Science/CFHTLS/>
- [20] URL <http://pswww.ifa.hawaii.edu/>
- [21] URL <http://www.darkenergysurvey.org/>
- [22] Tyson J A, Wittman D M and Angel J R P 2001 The Dark Matter Telescope *Gravitational Lensing: Recent Progress and Future Go (ASP Conf. Series vol 237)* ed Brainerd T G and Kochanek C S p 417 (*Preprint astro-ph/0005381*)
- [23] Tyson J A 1998 Dark Matter Tomography *SLAC Summer Institute 1998: Gravity from the Planck Era to the Present* SLAC/DOE Pub. SLAC-R-538 pp 89–112 URL [http://www.slac.stanford.edu/gen/meeting/ssi/1998/manu\\_list.html](http://www.slac.stanford.edu/gen/meeting/ssi/1998/manu_list.html)
- [24] National Research Council 2001 *Astronomy and Astrophysics in the New Millennium* (Washington DC: National Academies Press) ISBN 9780309073127 URL <https://doi.org/10.17226/9839>
- [25] Strauss M A 2004 *Report of the Science Working Group of the LSST prepared under the auspices of NOAO*
- [26] Tyson J A and Angel R 2001 The Large-aperture Synoptic Survey Telescope: Overview *The New Era of Wide Field Astronomy (ASP Conf. Series vol 232)* ed Clowes R, Adamson A and Bromage G p 347
- [27] Starr B M, Claver C F, Wolff S, Tyson J A, Lesser M P, Daggert L G, Dominguez R, Gomez Jr R R and Muller G P 2002 LSST Instrument Concept *Survey and Other Telescope Technologies and Discoveries (Proc. SPIE vol 4836)* ed Tyson J A and Wolff S pp 228–239
- [28] Tyson J A 2002 Large Synoptic Survey Telescope: Overview *Survey and Other Telescope Technologies and Discoveries (Proc. SPIE vol 4836)* ed Tyson J A and Wolff S pp 10–20 (*Preprint astro-ph/0302102*)
- [29] Angel R, Lesser M, Sarlot R and Dunham E 2000 Design for an 8-m Telescope with a 3 Degree Field at f/1.25: The Dark Matter Telescope *Imaging the Universe in Three Dimensions (ASP Conf. Series vol 195)* ed van Breugel W and Bland-Hawthorn J p 81

- [30] LSST Science Collaborations: Abell P A *et al* 2009 *LSST Science Book* (Preprint [0912.0201](#))
- [31] Albrecht A *et al* 2006 Report of the Dark Energy Task Force *ArXiv Astrophysics e-prints* (Preprint [astro-ph/0609591](#))
- [32] Ivezić Z *et al* for the LSST Collaboration 2008 LSST: from Science Drivers to Reference Design and Anticipated Data Products *ArXiv e-prints* (Preprint [0805.2366](#))
- [33] LSST Dark Energy Science Collaboration: Alexandra A *et al* 2012 Large Synoptic Survey Telescope: Dark Energy Science Collaboration *ArXiv e-prints* (Preprint [1211.0310](#))
- [34] Friedmann A 1922 Über die Krümmung des Raumes *Zeitschrift für Phys.* **10** 377–386
- [35] Lemaître G 1927 Un Univers homogène de masse constante et de rayon croissant rendant compte de la vitesse radiale des nébuleuses extra-galactiques *Annales de la Societe Scientifique de Bruxelles* **47** 49–59
- [36] Robertson H P 1935 Kinematics and World-Structure *Astrophys. J.* **82** 284
- [37] Walker A G 1935 On the formal comparison of Milne’s kinematical system with the systems of general relativity *Mon. Not. Roy. Astron. Soc.* **95** 263–269
- [38] Etherington I M H 1933 On the Definition of Distance in General Relativity. *Philosophical Magazine* **15** 761
- [39] Bassett B A and Kunz M 2004 Cosmic distance-duality as a probe of exotic physics and acceleration *Phys. Rev. D* **69** 101305 (Preprint [astro-ph/0312443](#))
- [40] Uzan J P, Aghanim N and Mellier Y 2004 Distance duality relation from x-ray and Sunyaev-Zel’dovich observations of clusters *Phys. Rev. D* **70** 083533 (Preprint [astro-ph/0405620](#))
- [41] Linder E V 2005 Cosmic growth history and expansion history *Phys. Rev. D* **72** 043529 (Preprint [astro-ph/0507263](#))
- [42] Knox L, Song Y S and Tyson J A 2006 Distance-redshift and growth-redshift relations as two windows on acceleration and gravitation: Dark energy or new gravity? *Phys. Rev. D* **74** 023512 (Preprint [astro-ph/0503644](#))
- [43] Ishak M, Upadhye A and Spergel D N 2006 Probing cosmic acceleration beyond the equation of state: Distinguishing between dark energy and modified gravity models *Phys. Rev. D* **74** 043513 (Preprint [astro-ph/0507184](#))
- [44] Peebles P J E 1980 *The Large-Scale Structure of the Universe* (Princeton University Press) ISBN 0691082405
- [45] Lightman A P and Schechter P L 1990 The Omega dependence of peculiar velocities induced by spherical density perturbations *Astrophys. J. Supp.* **74** 831
- [46] Lahav O, Lilje P B, Primack J R and Rees M J 1991 Dynamical effects of the cosmological constant *Mon. Not. Roy. Astron. Soc.* **251** 128–136
- [47] Wang L and Steinhardt P J 1998 Cluster Abundance Constraints for Cosmological Models with a Time-varying, Spatially Inhomogeneous Energy Component with Negative Pressure *Astrophys. J.* **508** 483–490 (Preprint [astro-ph/9804015](#))
- [48] White S D M 1979 The hierarchy of correlation functions and its relation to other measures of galaxy clustering *Mon. Not. Roy. Astron. Soc.* **186** 145–154
- [49] Szapudi I and Szalay A S 1993 Higher order statistics of the galaxy distribution using generating functions *Astrophys. J.* **408** 43–56

- [50] Takada M and Jain B 2003 The three-point correlation function in cosmology *Mon. Not. Roy. Astron. Soc.* **340** 580–608 (*Preprint* [astro-ph/0209167](#))
- [51] Wagner C, Müller V and Steinmetz M 2008 Constraining dark energy via baryon acoustic oscillations in the (an)isotropic light-cone power spectrum *Astron. & Astrophys.* **487** 63–74 (*Preprint* [0705.0354](#))
- [52] Kim J, Park C, Gott III J R and Dubinski J 2009 The Horizon Run N-Body Simulation: Baryon Acoustic Oscillations and Topology of Large-scale Structure of the Universe *Astrophys. J.* **701** 1547 (*Preprint* [0812.1392](#))
- [53] Blanton M, Cen R, Ostriker J P, Strauss M A and Tegmark M 2000 Time Evolution of Galaxy Formation and Bias in Cosmological Simulations *Astrophys. J.* **531** 1–16 (*Preprint* [astro-ph/9903165](#))
- [54] Somerville R S, Lemson G, Sigad Y, Dekel A, Kauffmann G and White S D M 2001 Non-linear stochastic galaxy biasing in cosmological simulations *Mon. Not. Roy. Astron. Soc.* **320** 289–306 (*Preprint* [astro-ph/9912073](#))
- [55] Weinberg D H, Davé R, Katz N and Hernquist L 2004 Galaxy Clustering and Galaxy Bias in a  $\Lambda$ CDM Universe *Astrophys. J.* **601** 1–21 (*Preprint* [astro-ph/0212356](#))
- [56] Tinker J L, Robertson B E, Kravtsov A V, Klypin A, Warren M S, Yepes G and Gottlöber S 2010 The Large-scale Bias of Dark Matter Halos: Numerical Calibration and Model Tests *Astrophys. J.* **724** 878–886 (*Preprint* [1001.3162](#))
- [57] Manera M, Sheth R K and Scoccimarro R 2010 Large-scale bias and the inaccuracy of the peak-background split *Mon. Not. Roy. Astron. Soc.* **402** 589–602 (*Preprint* [0906.1314](#))
- [58] Wang Q and Zhan H 2013 Mass-dependent Baryon Acoustic Oscillation Signal and Halo Bias *Astrophys. J. Lett.* **768** L27 (*Preprint* [1302.1640](#))
- [59] Cole S and Kaiser N 1989 Biased clustering in the cold dark matter cosmogony *Mon. Not. Roy. Astron. Soc.* **237** 1127–1146
- [60] Mo H J and White S D M 1996 An analytic model for the spatial clustering of dark matter haloes *Mon. Not. Roy. Astron. Soc.* **282** 347–361 (*Preprint* [astro-ph/9512127](#))
- [61] Catelan P, Lucchin F, Matarrese S and Porciani C 1998 The bias field of dark matter haloes *Mon. Not. Roy. Astron. Soc.* **297** 692–712 (*Preprint* [astro-ph/9708067](#))
- [62] Sheth R K and Tormen G 1999 Large-scale bias and the peak background split *Mon. Not. Roy. Astron. Soc.* **308** 119–126 (*Preprint* [astro-ph/9901122](#))
- [63] Hu W and Jain B 2004 Joint galaxy-lensing observables and the dark energy *Phys. Rev. D* **70** 043009 (*Preprint* [astro-ph/0312395](#))
- [64] Zheng Z and Weinberg D H 2007 Breaking the Degeneracies between Cosmology and Galaxy Bias *Astrophys. J.* **659** 1–28 (*Preprint* [astro-ph/0512071](#))
- [65] Cacciato M, Lahav O, van den Bosch F C, Hoekstra H and Dekel A 2012 On combining galaxy clustering and weak lensing to unveil galaxy biasing via the halo model *Mon. Not. Roy. Astron. Soc.* **426** 566–587 (*Preprint* [1203.2616](#))
- [66] Feldman H A, Kaiser N and Peacock J A 1994 Power-spectrum analysis of three-dimensional redshift surveys *Astrophys. J.* **426** 23–37 (*Preprint* [astro-ph/9304022](#))
- [67] Vogeley M S and Szalay A S 1996 Eigenmode Analysis of Galaxy Redshift Surveys. I. Theory and Methods *Astrophys. J.* **465** 34 (*Preprint* [astro-ph/9601185](#))
- [68] Hamilton A J S and Tegmark M 2000 Decorrelating the power spectrum of galaxies *Mon. Not. Roy. Astron. Soc.* **312** 285–294 (*Preprint* [astro-ph/9905192](#))

- [69] Peacock J A and Smith R E 2000 Halo occupation numbers and galaxy bias *Mon. Not. Roy. Astron. Soc.* **318** 1144–1156 (*Preprint* [astro-ph/0005010](#))
- [70] Scoccimarro R, Sheth R K, Hui L and Jain B 2001 How Many Galaxies Fit in a Halo? Constraints on Galaxy Formation Efficiency from Spatial Clustering *Astrophys. J.* **546** 20–34 (*Preprint* [astro-ph/0006319](#))
- [71] Marinoni C et al 2005 The VIMOS VLT Deep Survey. Evolution of the non-linear galaxy bias up to  $z = 1.5$  *Astron. & Astrophys.* **442** 801–825 (*Preprint* [astro-ph/0506561](#))
- [72] Seljak U et al 2005 SDSS galaxy bias from halo mass-bias relation and its cosmological implications *Phys. Rev. D* **71** 043511 (*Preprint* [astro-ph/0406594](#))
- [73] Blanton M R, Eisenstein D, Hogg D W and Zehavi I 2006 The Scale Dependence of Relative Galaxy Bias: Encouragement for the “Halo Model” Description *Astrophys. J.* **645** 977–985 (*Preprint* [astro-ph/0411037](#))
- [74] Marín F A et al 2013 The WiggleZ Dark Energy Survey: constraining galaxy bias and cosmic growth with three-point correlation functions *Mon. Not. Roy. Astron. Soc.* **432** 2654–2668 (*Preprint* [1303.6644](#))
- [75] Crocce M and Scoccimarro R 2006 Renormalized cosmological perturbation theory *Phys. Rev. D* **73** 063519 (*Preprint* [astro-ph/0509418](#))
- [76] Jeong D and Komatsu E 2006 Perturbation Theory Reloaded: Analytical Calculation of Nonlinearity in Baryonic Oscillations in the Real-Space Matter Power Spectrum *Astrophys. J.* **651** 619–626 (*Preprint* [astro-ph/0604075](#))
- [77] McDonald P 2007 Dark matter clustering: A simple renormalization group approach *Phys. Rev. D* **75** 043514 (*Preprint* [astro-ph/0606028](#))
- [78] Matarrese S and Pietroni M 2007 Resumming cosmic perturbations *J. Cosmo. Astropart. Phys.* **6** 026 (*Preprint* [astro-ph/0703563](#))
- [79] Matsubara T 2008 Nonlinear perturbation theory with halo bias and redshift-space distortions via the Lagrangian picture *Phys. Rev. D* **78** 083519 (*Preprint* [0807.1733](#))
- [80] Pietroni M 2008 Flowing with time: a new approach to non-linear cosmological perturbations *J. Cosmo. Astropart. Phys.* **10** 036 (*Preprint* [0806.0971](#))
- [81] Taruya A, Bernardeau F, Nishimichi T and Codis S 2012 Direct and fast calculation of regularized cosmological power spectrum at two-loop order *Phys. Rev. D* **86** 103528 (*Preprint* [1208.1191](#))
- [82] Heitmann K, White M, Wagner C, Habib S and Higdon D 2010 The Coyote Universe. I. Precision Determination of the Nonlinear Matter Power Spectrum *Astrophys. J.* **715** 104–121 (*Preprint* [0812.1052](#))
- [83] Huterer D and Takada M 2005 Calibrating the nonlinear matter power spectrum: Requirements for future weak lensing surveys *Astroparticle Physics* **23** 369–376 (*Preprint* [astro-ph/0412142](#))
- [84] Hearin A P, Zentner A R and Ma Z 2012 General requirements on matter power spectrum predictions for cosmology with weak lensing tomography *J. Cosmo. Astropart. Phys.* **4** 034 (*Preprint* [1111.0052](#))
- [85] Heitmann K, Higdon D, White M, Habib S, Williams B J, Lawrence E and Wagner C 2009 The Coyote Universe. II. Cosmological Models and Precision Emulation of the Nonlinear Matter Power Spectrum *Astrophys. J.* **705** 156–174 (*Preprint* [0902.0429](#))

- [86] Lawrence E, Heitmann K, White M, Higdon D, Wagner C, Habib S and Williams B 2010 The Coyote Universe. III. Simulation Suite and Precision Emulator for the Nonlinear Matter Power Spectrum *Astrophys. J.* **713** 1322–1331 (*Preprint* [0912.4490](#))
- [87] Agarwal S, Abdalla F B, Feldman H A, Lahav O and Thomas S A 2012 PkANN - I. Non-linear matter power spectrum interpolation through artificial neural networks *Mon. Not. Roy. Astron. Soc.* **424** 1409–1418 (*Preprint* [1203.1695](#))
- [88] Agarwal S, Abdalla F B, Feldman H A, Lahav O and Thomas S A 2014 PkANN - II. A non-linear matter power spectrum interpolator developed using artificial neural networks *Mon. Not. Roy. Astron. Soc.* **439** 2102–2121 (*Preprint* [1312.2101](#))
- [89] Peacock J A and Dodds S J 1996 Non-linear evolution of cosmological power spectra *Mon. Not. Roy. Astron. Soc.* **280** L19–L26 (*Preprint* [astro-ph/9603031](#))
- [90] Smith R E, Peacock J A, Jenkins A, White S D M, Frenk C S, Pearce F R, Thomas P A, Efstathiou G and Couchman H M P 2003 Stable clustering, the halo model and non-linear cosmological power spectra *Mon. Not. Roy. Astron. Soc.* **341** 1311–1332 (*Preprint* [astro-ph/0207664](#))
- [91] Takahashi R, Sato M, Nishimichi T, Taruya A and Oguri M 2012 Revising the Halofit Model for the Nonlinear Matter Power Spectrum *Astrophys. J.* **761** 152 (*Preprint* [1208.2701](#))
- [92] Caldwell R R and Kamionkowski M 2009 The Physics of Cosmic Acceleration *Annual Review of Nuclear and Particle Science* **59** 397–429 (*Preprint* [0903.0866](#))
- [93] Clifton T, Ferreira P G, Padilla A and Skordis C 2012 Modified gravity and cosmology *Phys. Rep.* **513** 1–189 (*Preprint* [1106.2476](#))
- [94] Koyama K 2016 Cosmological tests of modified gravity *Reports on Progress in Physics* **79** 046902 (*Preprint* [1504.04623](#))
- [95] Buchert T and Ehlers J 1997 Averaging inhomogeneous Newtonian cosmologies. *Astron. & Astrophys.* **320** 1–7 (*Preprint* [astro-ph/9510056](#))
- [96] Clarkson C, Ellis G, Larena J and Umeh O 2011 Does the growth of structure affect our dynamical models of the universe? the averaging, backreaction, and fitting problems in cosmology *Reports on Progress in Physics* **74** 112901 (*Preprint* [1109.2314](#)) URL <http://stacks.iop.org/0034-4885/74/i=11/a=112901>
- [97] Buchert T and Räsänen S 2012 Backreaction in Late-Time Cosmology *Annual Review of Nuclear and Particle Science* **62** 57–79 (*Preprint* [1112.5335](#))
- [98] Robertson H P 1955 The Theoretical Aspects of the Nebular Redshift *Pub. Astron. Soc. Pacific* **67** 82
- [99] Hoyle F and Sandage A 1956 The Second-Order Term in the Redshift-Magnitude Relation *Pub. Astron. Soc. Pacific* **68** 301
- [100] Turner M S and Riess A G 2002 Do Type Ia Supernovae Provide Direct Evidence for Past Deceleration of the Universe? *Astrophys. J.* **569** 18–22 (*Preprint* [astro-ph/0106051](#))
- [101] Shapiro C and Turner M S 2006 What Do We Really Know about Cosmic Acceleration? *Astrophys. J.* **649** 563–569 (*Preprint* [astro-ph/0512586](#))
- [102] Neben A R and Turner M S 2013 Beyond  $H_0$  and  $q_0$ : Cosmology is No Longer Just Two Numbers *Astrophys. J.* **769** 133 (*Preprint* [1209.0480](#))
- [103] Sandage A 1962 The Change of Redshift and Apparent Luminosity of Galaxies due to the Deceleration of Selected Expanding Universes. *Astrophys. J.* **136** 319–+

- [104] McVittie G C 1962 Appendix to The Change of Redshift and Apparent Luminosity of Galaxies due to the Deceleration of Selected Expanding Universes. *Astrophys. J.* **136** 334
- [105] Linder E V 1997 *First Principles of Cosmology* (Prentice Hall) ISBN 0201403951
- [106] Loeb A 1998 Direct Measurement of Cosmological Parameters from the Cosmic Deceleration of Extragalactic Objects *Astrophys. J. Lett.* **499** L111+ (*Preprint astro-ph/9802122*)
- [107] Jimenez R and Loeb A 2002 Constraining Cosmological Parameters Based on Relative Galaxy Ages *Astrophys. J.* **573** 37–42 (*Preprint astro-ph/0106145*)
- [108] Moresco M et al 2012 Improved constraints on the expansion rate of the Universe up to  $z \sim 1.1$  from the spectroscopic evolution of cosmic chronometers *J. Cosmo. Astropart. Phys.* **8** 006 (*Preprint 1201.3609*)
- [109] Tomita K 2001 A local void and the accelerating Universe *Mon. Not. Roy. Astron. Soc.* **326** 287–292 (*Preprint astro-ph/0011484*)
- [110] Alnes H, Amarsguioi M and Grøn Ø 2006 Inhomogeneous alternative to dark energy? *Phys. Rev. D* **73** 083519 (*Preprint astro-ph/0512006*)
- [111] Biswas T, Mansouri R and Notari A 2007 Non-linear structure formation and ‘apparent’ acceleration: an investigation *J. Cosmo. Astropart. Phys.* **12** 017 (*Preprint astro-ph/0606703*)
- [112] Moss A, Zibin J P and Scott D 2011 Precision cosmology defeats void models for acceleration *Phys. Rev. D* **83** 103515 (*Preprint 1007.3725*)
- [113] Zhang P and Stebbins A 2011 Confirmation of the Copernican Principle at Gpc Radial Scale and above from the Kinetic Sunyaev-Zel’dovich Effect Power Spectrum *Physical Review Letters* **107** 041301 (*Preprint 1009.3967*)
- [114] Buchert T 2000 On Average Properties of Inhomogeneous Fluids in General Relativity: Dust Cosmologies *General Relativity and Gravitation* **32** 105–126 (*Preprint gr-qc/9906015*)
- [115] Räsänen S 2004 Dark energy from back-reaction *J. Cosmo. Astropart. Phys.* **2** 003 (*Preprint astro-ph/0311257*)
- [116] Ellis G F R and Buchert T 2005 The universe seen at different scales [rapid communication] *Physics Letters A* **347** 38–46 (*Preprint gr-qc/0506106*)
- [117] Kolb E W, Matarrese S and Riotto A 2006 On cosmic acceleration without dark energy *New Journal of Physics* **8** 322 (*Preprint astro-ph/0506534*)
- [118] Siegel E R and Fry J N 2005 The Effects of Inhomogeneities on Cosmic Expansion *Astrophys. J. Lett.* **628** L1–L4 (*Preprint astro-ph/0504421*)
- [119] Kasai M, Asada H and Futamase T 2006 Toward a No-Go Theorem for an Accelerating Universe through a Nonlinear Backreaction *Progress of Theoretical Physics* **115** 827–832 (*Preprint astro-ph/0602506*)
- [120] Baumann D, Nicolis A, Senatore L and Zaldarriaga M 2012 Cosmological non-linearities as an effective fluid *J. Cosmo. Astropart. Phys.* **7** 051 (*Preprint 1004.2488*)
- [121] Gunn J E and Tinsley B M 1975 An accelerating Universe *Nature* **257** 454–457
- [122] Peebles P J E 1984 Tests of cosmological models constrained by inflation *Astrophys. J.* **284** 439–444

- [123] Efstathiou G, Sutherland W J and Maddox S J 1990 The cosmological constant and cold dark matter *Nature* **348** 705–707
- [124] Ostriker J P and Steinhardt P J 1995 The observational case for a low-density Universe with a non-zero cosmological constant *Nature* **377** 600–602
- [125] Krauss L M and Turner M S 1995 The cosmological constant is back *General Relativity and Gravitation* **27** 1137–1144 (Preprint [astro-ph/9504003](#))
- [126] Peebles P J E and Ratra B 1988 Cosmology with a time-variable cosmological 'constant' *Astrophys. J. Lett.* **325** L17–L20
- [127] Zlatev I, Wang L and Steinhardt P J 1999 Quintessence, Cosmic Coincidence, and the Cosmological Constant *Physical Review Letters* **82** 896–899 (Preprint [astro-ph/9807002](#))
- [128] Chiba T, Okabe T and Yamaguchi M 2000 Kinetically driven quintessence *Phys. Rev. D* **62** 023511 (Preprint [astro-ph/9912463](#))
- [129] Feng B, Wang X and Zhang X 2005 Dark energy constraints from the cosmic age and supernova *Physics Letters B* **607** 35–41 (Preprint [astro-ph/0404224](#))
- [130] Silvestri A and Trodden M 2009 Approaches to understanding cosmic acceleration *Reports on Progress in Physics* **72** 096901 (Preprint [0904.0024](#))
- [131] Chevallier M and Polarski D 2001 Accelerating Universes with Scaling Dark Matter *International Journal of Modern Physics D* **10** 213–223 (Preprint [gr-qc/0009008](#))
- [132] Linder E V 2003 Exploring the Expansion History of the Universe *Physical Review Letters* **90** 091301 (Preprint [astro-ph/0208512](#))
- [133] Albrecht A and Bernstein G 2007 Evaluating dark energy probes using multidimensional dark energy parameters *Phys. Rev. D* **75** 103003 (Preprint [astro-ph/0608269](#))
- [134] Albrecht A et al 2009 Findings of the Joint Dark Energy Mission Figure of Merit Science Working Group *ArXiv e-prints* (Preprint [0901.0721](#))
- [135] Armendariz-Picon C, Mukhanov V and Steinhardt P J 2000 Dynamical Solution to the Problem of a Small Cosmological Constant and Late-Time Cosmic Acceleration *Physical Review Letters* **85** 4438 (Preprint [astro-ph/0004134](#))
- [136] Erickson J K, Caldwell R R, Steinhardt P J, Armendariz-Picon C and Mukhanov V 2002 Measuring the Speed of Sound of Quintessence *Physical Review Letters* **88** 121301 (Preprint [astro-ph/0112438](#))
- [137] Bean R and Doré O 2004 Probing dark energy perturbations: The dark energy equation of state and speed of sound as measured by WMAP *Phys. Rev. D* **69** 083503 (Preprint [astro-ph/0307100](#))
- [138] Hu W and Scranton R 2004 Measuring dark energy clustering with CMB-galaxy correlations *Phys. Rev. D* **70** 123002 (Preprint [astro-ph/0408456](#))
- [139] Dvali G, Gabadadze G and Porrati M 2000 4D gravity on a brane in 5D Minkowski space *Physics Letters B* **485** 208–214 (Preprint [hep-th/0005016](#))
- [140] Capozziello S 2002 Curvature Quintessence *International Journal of Modern Physics D* **11** 483–491 (Preprint [gr-qc/0201033](#))
- [141] Carroll S M, Duvvuri V, Trodden M and Turner M S 2004 Is cosmic speed-up due to new gravitational physics? *Phys. Rev. D* **70** 043528 (Preprint [astro-ph/0306438](#))
- [142] Song Y S, Sawicki I and Hu W 2007 Large-scale tests of the Dvali-Gabadadze-Porrati model *Phys. Rev. D* **75** 064003 (Preprint [astro-ph/0606286](#))

- [143] Jain B, Vikram V and Sakstein J 2013 Astrophysical Tests of Modified Gravity: Constraints from Distance Indicators in the Nearby Universe *Astrophys. J.* **779** 39 (Preprint [1204.6044](#))
- [144] Deffayet C 2001 Cosmology on a brane in Minkowski bulk *Physics Letters B* **502** 199–208 (Preprint [hep-th/0010186](#))
- [145] Lue A 2006 The phenomenology of Dvali Gabadadze Porrati cosmologies *Phys. Rep.* **423** 1–48 (Preprint [astro-ph/0510068](#))
- [146] Kunz M and Sapone D 2007 Dark Energy versus Modified Gravity *Physical Review Letters* **98** 121301 (Preprint [astro-ph/0612452](#))
- [147] Bertschinger E and Zukin P 2008 Distinguishing modified gravity from dark energy *Phys. Rev. D* **78** 024015 (Preprint [0801.2431](#))
- [148] Jain B and Zhang P 2008 Observational tests of modified gravity *Phys. Rev. D* **78** 063503 (Preprint [0709.2375](#))
- [149] Planck Collaboration: Ade P A R *et al* 2016 Planck 2015 results. XIII. Cosmological parameters *Astron. & Astrophys.* **594** A13 (Preprint [1502.01589](#))
- [150] Hu W and Haiman Z 2003 Redshifting rings of power *Phys. Rev. D* **68** 063004 (Preprint [astro-ph/0306053](#))
- [151] Linder E V 2003 Baryon oscillations as a cosmological probe *Phys. Rev. D* **68** 083504 (Preprint [astro-ph/0304001](#))
- [152] Seo H J and Eisenstein D J 2003 Probing Dark Energy with Baryonic Acoustic Oscillations from Future Large Galaxy Redshift Surveys *Astrophys. J.* **598** 720–740 (Preprint [astro-ph/0307460](#))
- [153] Gaztañaga E, Miquel R and Sánchez E 2009 First Cosmological Constraints on Dark Energy from the Radial Baryon Acoustic Scale *Physical Review Letters* **103** 091302 (Preprint [0808.1921](#))
- [154] Sánchez E, Alonso D, Sánchez F J, García-Bellido J and Sevilla I 2013 Precise measurement of the radial baryon acoustic oscillation scales in galaxy redshift surveys *Mon. Not. Roy. Astron. Soc.* **434** 2008–2019 (Preprint [1210.6446](#))
- [155] Kaiser N 1987 Clustering in real space and in redshift space *Mon. Not. Roy. Astron. Soc.* **227** 1–21
- [156] Peacock J A *et al* 2001 A measurement of the cosmological mass density from clustering in the 2dF Galaxy Redshift Survey *Nature* **410** 169–173 (Preprint [astro-ph/0103143](#))
- [157] Guzzo L *et al* 2008 A test of the nature of cosmic acceleration using galaxy redshift distortions *Nature* **451** 541–544 (Preprint [0802.1944](#))
- [158] Alam S *et al* 2017 The clustering of galaxies in the completed SDSS-III Baryon Oscillation Spectroscopic Survey: cosmological analysis of the DR12 galaxy sample *Mon. Not. Roy. Astron. Soc.* **470** 2617–2652 (Preprint [1607.03155](#))
- [159] Zhan H, Knox L and Tyson J A 2009 Distance, Growth Factor, and Dark Energy Constraints from Photometric Baryon Acoustic Oscillation and Weak Lensing Measurements *Astrophys. J.* **690** 923–936 (Preprint [0806.0937](#))
- [160] Schlegel D *et al* 2011 The BigBOSS Experiment *ArXiv e-prints* (Preprint [1106.1706](#))
- [161] Amendola L *et al* 2013 Cosmology and Fundamental Physics with the Euclid Satellite *Living Reviews in Relativity* **16** 6 (Preprint [1206.1225](#))

- [162] Zwicky F 1933 Die Rotverschiebung von extragalaktischen Nebeln *Helvetica Physica Acta* **6** 110–127
- [163] Rubin V C, Thonnard N and Ford Jr W K 1978 Extended rotation curves of high-luminosity spiral galaxies. IV - Systematic dynamical properties, SA through SC *Astrophys. J. Lett.* **225** L107–L111
- [164] Faber S M and Gallagher J S 1979 Masses and mass-to-light ratios of galaxies *Ann. Rev. Astron. & Astrophys.* **17** 135–187
- [165] Fabricant D, Lecar M and Gorenstein P 1980 X-ray measurements of the mass of M87 *Astrophys. J.* **241** 552–560
- [166] Kriss G A, Cioffi D F and Canizares C R 1983 The X-ray emitting gas in poor clusters with central dominant galaxies *Astrophys. J.* **272** 439–448
- [167] Clowe D, Gonzalez A and Markevitch M 2004 Weak-Lensing Mass Reconstruction of the Interacting Cluster 1E 0657-558: Direct Evidence for the Existence of Dark Matter *Astrophys. J.* **604** 596–603 (*Preprint* [astro-ph/0312273](#))
- [168] Blumenthal G R, Faber S M, Primack J R and Rees M J 1984 Formation of galaxies and large-scale structure with cold dark matter *Nature* **311** 517–525
- [169] Bertone G, Hooper D and Silk J 2005 Particle dark matter: evidence, candidates and constraints *Phys. Rep.* **405** 279–390 (*Preprint* [hep-ph/0404175](#))
- [170] Feng J L 2010 Dark Matter Candidates from Particle Physics and Methods of Detection *Ann. Rev. Astron. & Astrophys.* **48** 495–545 (*Preprint* [1003.0904](#))
- [171] Bahcall N A, Fan X and Cen R 1997 Constraining  $\Omega$  with Cluster Evolution *Astrophys. J. Lett.* **485** L53–L56 (*Preprint* [astro-ph/9706018](#))
- [172] Hinshaw G *et al* 2013 Nine-year Wilkinson Microwave Anisotropy Probe (WMAP) Observations: Cosmological Parameter Results *Astrophys. J. Supp.* **208** 19 (*Preprint* [1212.5226](#))
- [173] Zhan H, Knox L, Tyson J A and Margoniner V 2006 Exploring Large-Scale Structure with Billions of Galaxies *Astrophys. J.* **640** 8–17 (*Preprint* [astro-ph/0508119](#))
- [174] Zhan H 2006 Cosmic tomographies: baryon acoustic oscillations and weak lensing *Journal of Cosmology and Astro-Particle Physics* **8** 8–+ (*Preprint* [astro-ph/0605696](#))
- [175] Blas D, Lesgourgues J and Tram T 2011 The Cosmic Linear Anisotropy Solving System (CLASS). Part II: Approximation schemes *J. Cosmo. Astropart. Phys.* **7** 034 (*Preprint* [1104.2933](#))
- [176] Peebles P J E and Yu J T 1970 Primeval Adiabatic Perturbation in an Expanding Universe *Astrophys. J.* **162** 815–+
- [177] Bond J R and Efstathiou G 1984 Cosmic background radiation anisotropies in universes dominated by nonbaryonic dark matter *Astrophys. J. Lett.* **285** L45–L48
- [178] Holtzman J A 1989 Microwave background anisotropies and large-scale structure in universes with cold dark matter, baryons, radiation, and massive and massless neutrinos *Astrophys. J. Supp.* **71** 1–24
- [179] Klypin A, Kravtsov A V, Valenzuela O and Prada F 1999 Where Are the Missing Galactic Satellites? *Astrophys. J.* **522** 82–92 (*Preprint* [astro-ph/9901240](#))
- [180] Moore B, Ghigna S, Governato F, Lake G, Quinn T, Stadel J and Tozzi P 1999 Dark Matter Substructure within Galactic Halos *Astrophys. J. Lett.* **524** L19–L22 (*Preprint* [astro-ph/9907411](#))

- [181] Moore B, Quinn T, Governato F, Stadel J and Lake G 1999 Cold collapse and the core catastrophe *Mon. Not. Roy. Astron. Soc.* **310** 1147–1152 (*Preprint* [astro-ph/9903164](#))
- [182] Navarro J F, Hayashi E, Power C, Jenkins A R, Frenk C S, White S D M, Springel V, Stadel J and Quinn T R 2004 The inner structure of  $\Lambda$ CDM haloes - III. Universality and asymptotic slopes *Mon. Not. Roy. Astron. Soc.* **349** 1039–1051 (*Preprint* [astro-ph/0311231](#))
- [183] Gilmore G, Wilkinson M I, Wyse R F G, Kleyna J T, Koch A, Evans N W and Grebel E K 2007 The Observed Properties of Dark Matter on Small Spatial Scales *Astrophys. J.* **663** 948–959 (*Preprint* [astro-ph/0703308](#))
- [184] Kuzio de Naray R, McGaugh S S and de Blok W J G 2008 Mass Models for Low Surface Brightness Galaxies with High-Resolution Optical Velocity Fields *Astrophys. J.* **676** 920–943 (*Preprint* [0712.0860](#))
- [185] Boylan-Kolchin M, Bullock J S and Kaplinghat M 2011 Too big to fail? The puzzling darkness of massive Milky Way subhaloes *Mon. Not. Roy. Astron. Soc.* **415** L40–L44 (*Preprint* [1103.0007](#))
- [186] Governato F, Zolotov A, Pontzen A, Christensen C, Oh S H, Brooks A M, Quinn T, Shen S and Wadsley J 2012 Cuspy no more: how outflows affect the central dark matter and baryon distribution in  $\Lambda$  cold dark matter galaxies *Mon. Not. Roy. Astron. Soc.* **422** 1231–1240 (*Preprint* [1202.0554](#))
- [187] Bode P, Ostriker J P and Turok N 2001 Halo Formation in Warm Dark Matter Models *Astrophys. J.* **556** 93–107 (*Preprint* [astro-ph/0010389](#))
- [188] Spergel D N and Steinhardt P J 2000 Observational Evidence for Self-Interacting Cold Dark Matter *Physical Review Letters* **84** 3760–3763 (*Preprint* [astro-ph/9909386](#))
- [189] Lin W B, Huang D H, Zhang X and Brandenberger R 2001 Nonthermal Production of Weakly Interacting Massive Particles and the Subgalactic Structure of the Universe *Physical Review Letters* **86** 954–957 (*Preprint* [astro-ph/0009003](#))
- [190] Bovy J and Tremaine S 2012 On the Local Dark Matter Density *Astrophys. J.* **756** 89 (*Preprint* [1205.4033](#))
- [191] Viel M, Becker G D, Bolton J S, Haehnelt M G, Rauch M and Sargent W L W 2008 How Cold Is Cold Dark Matter? Small-Scales Constraints from the Flux Power Spectrum of the High-Redshift Lyman- $\alpha$  Forest *Physical Review Letters* **100** 041304 (*Preprint* [0709.0131](#))
- [192] Markevitch M, Gonzalez A H, David L, Vikhlinin A, Murray S, Forman W, Jones C and Tucker W 2002 A Textbook Example of a Bow Shock in the Merging Galaxy Cluster 1E 0657-56 *Astrophys. J. Lett.* **567** L27–L31 (*Preprint* [astro-ph/0110468](#))
- [193] Markevitch M, Gonzalez A H, Clowe D, Vikhlinin A, Forman W, Jones C, Murray S and Tucker W 2004 Direct Constraints on the Dark Matter Self-Interaction Cross Section from the Merging Galaxy Cluster 1E 0657-56 *Astrophys. J.* **606** 819–824 (*Preprint* [astro-ph/0309303](#))
- [194] Robertson A, Massey R and Eke V 2017 What does the Bullet Cluster tell us about self-interacting dark matter? *Mon. Not. Roy. Astron. Soc.* **465** 569–587 (*Preprint* [1605.04307](#))
- [195] Bond J R, Efstathiou G and Silk J 1980 Massive neutrinos and the large-scale structure of the universe *Physical Review Letters* **45** 1980–1984

- [196] Ma C P and Bertschinger E 1995 Cosmological Perturbation Theory in the Synchronous and Conformal Newtonian Gauges *Astrophys. J.* **455** 7 (*Preprint* [astro-ph/9506072](#))
- [197] King S F and Luhn C 2013 Neutrino mass and mixing with discrete symmetry *Reports on Progress in Physics* **76** 056201 (*Preprint* [1301.1340](#))
- [198] de Bernardis F, Kitching T D, Heavens A and Melchiorri A 2009 Determining the neutrino mass hierarchy with cosmology *Phys. Rev. D* **80** 123509 (*Preprint* [0907.1917](#))
- [199] Hannestad S and Schwetz T 2016 Cosmology and the neutrino mass ordering *J. Cosmo. Astropart. Phys.* **11** 035 (*Preprint* [1606.04691](#))
- [200] Vagnozzi S, Giusarma E, Mena O, Freese K, Gerbino M, Ho S and Lattanzi M 2017 Unveiling  $\nu$  secrets with cosmological data: Neutrino masses and mass hierarchy *Phys. Rev. D* **96** 123503 (*Preprint* [1701.08172](#))
- [201] Hu W, Eisenstein D J and Tegmark M 1998 Weighing Neutrinos with Galaxy Surveys *Physical Review Letters* **80** 5255–5258 (*Preprint* [astro-ph/9712057](#))
- [202] Lesgourgues J and Pastor S 2006 Massive neutrinos and cosmology *Phys. Rep.* **429** 307–379 (*Preprint* [astro-ph/0603494](#))
- [203] Ali-Haïmoud Y and Bird S 2013 An efficient implementation of massive neutrinos in non-linear structure formation simulations *Mon. Not. Roy. Astron. Soc.* **428** 3375–3389 (*Preprint* [1209.0461](#))
- [204] Carbone C, Petkova M and Dolag K 2016 DEMNUni: ISW, Rees-Sciama, and weak-lensing in the presence of massive neutrinos *J. Cosmo. Astropart. Phys.* **7** 034 (*Preprint* [1605.02024](#))
- [205] Zennaro M, Bel J, Villaescusa-Navarro F, Carbone C, Sefusatti E and Guzzo L 2017 Initial conditions for accurate N-body simulations of massive neutrino cosmologies *Mon. Not. Roy. Astron. Soc.* **466** 3244–3258 (*Preprint* [1605.05283](#))
- [206] Song Y S and Knox L 2004 Determination of cosmological parameters from cosmic shear data *Phys. Rev. D* **70** 063510 (*Preprint* [astro-ph/0312175](#))
- [207] Font-Ribera A, McDonald P, Mostek N, Reid B A, Seo H J and Slosar A 2014 DESI and other Dark Energy experiments in the era of neutrino mass measurements *J. Cosmo. Astropart. Phys.* **5** 023 (*Preprint* [1308.4164](#))
- [208] Lyth D H D H and Riotto A A 1999 Particle physics models of inflation and the cosmological density perturbation *Phys. Rep.* **314** 1–146 (*Preprint* [hep-ph/9807278](#))
- [209] Seljak U and Zaldarriaga M 1997 Signature of Gravity Waves in the Polarization of the Microwave Background *Physical Review Letters* **78** 2054–2057 (*Preprint* [astro-ph/9609169](#))
- [210] Kamionkowski M, Kosowsky A and Stebbins A 1997 A Probe of Primordial Gravity Waves and Vorticity *Physical Review Letters* **78** 2058–2061 (*Preprint* [astro-ph/9609132](#))
- [211] Hanson D *et al* 2013 Detection of B-Mode Polarization in the Cosmic Microwave Background with Data from the South Pole Telescope *Physical Review Letters* **111** 141301 (*Preprint* [1307.5830](#))
- [212] The Polarbear Collaboration: Ade P A R *et al* 2014 A Measurement of the Cosmic Microwave Background B-mode Polarization Power Spectrum at Sub-degree Scales with POLARBEAR *Astrophys. J.* **794** 171 (*Preprint* [1403.2369](#))

- [213] BICEP2 Collaboration, Keck Array Collaboration, Ade P A R and *et al* 2016 Improved Constraints on Cosmology and Foregrounds from BICEP2 and Keck Array Cosmic Microwave Background Data with Inclusion of 95 GHz Band *Physical Review Letters* **116** 031302 (*Preprint* [1510.09217](#))
- [214] Bartolo N, Komatsu E, Matarrese S and Riotto A 2004 Non-Gaussianity from inflation: theory and observations *Phys. Rep.* **402** 103–266 (*Preprint* [astro-ph/0406398](#))
- [215] Komatsu E *et al* 2009 Five-Year Wilkinson Microwave Anisotropy Probe Observations: Cosmological Interpretation *Astrophys. J. Supp.* **180** 330–376 (*Preprint* [0803.0547](#))
- [216] Planck Collaboration: Ade P A R *et al* 2016 Planck 2015 results. XVII. Constraints on primordial non-Gaussianity *Astron. & Astrophys.* **594** A17 (*Preprint* [1502.01592](#))
- [217] Alvarez M *et al* 2014 Testing Inflation with Large Scale Structure: Connecting Hopes with Reality *ArXiv e-prints* (*Preprint* [1412.4671](#))
- [218] Connolly A J *et al* 2014 An end-to-end simulation framework for the Large Synoptic Survey Telescope *Modeling, Systems Engineering, and Project Management for Astronomy VI (Proc. SPIE vol 9150)* p 915014
- [219] Jones R L, Yoachim P, Chandrasekharan S, Connolly A J, Cook K H, Ivezić Ž, Krughoff K S, Petry C and Ridgway S T 2014 The LSST metrics analysis framework (MAF) *Observatory Operations: Strategies, Processes, and Systems V (Proc. SPIE vol 9149)* p 91490B
- [220] URL <http://ls.st/srd>
- [221] Stubbs C W and Tonry J L 2006 Toward 1% Photometry: End-to-End Calibration of Astronomical Telescopes and Detectors *Astrophys. J.* **646** 1436–1444 (*Preprint* [astro-ph/0604285](#))
- [222] Stubbs C W, High F W, George M R, DeRose K L, Blondin S, Tonry J L, Chambers K C, Granett B R, Burke D L and Smith R C 2007 Toward More Precise Survey Photometry for PanSTARRS and LSST: Measuring Directly the Optical Transmission Spectrum of the Atmosphere *Pub. Astron. Soc. Pacific* **119** 1163–1178 (*Preprint* [0708.1364](#))
- [223] URL <http://ls.st/dpdd>
- [224] URL <http://www.ncsa.illinois.edu/enabling/data/lsst>
- [225] Myers A D, White M and Ball N M 2009 Incorporating photometric redshift probability density information into real-space clustering measurements *Mon. Not. Roy. Astron. Soc.* **399** 2279–2287 (*Preprint* [0903.3121](#))
- [226] Abrahamse A, Knox L, Schmidt S, Thorman P, Tyson J A and Zhan H 2011 Characterizing and Propagating Modeling Uncertainties in Photometrically Derived Redshift Distributions *Astrophys. J.* **734** 36 (*Preprint* [1011.2239](#))
- [227] Sheldon E S, Cunha C E, Mandelbaum R, Brinkmann J and Weaver B A 2012 Photometric Redshift Probability Distributions for Galaxies in the SDSS DR8 *Astrophys. J. Supp.* **201** 32 (*Preprint* [1109.5192](#))
- [228] Zhan H, Wang L, Pinto P and Tyson J A 2008 Measuring Baryon Acoustic Oscillations with Millions of Supernovae *Astrophys. J. Lett.* **675** L1–L4 (*Preprint* [0801.3659](#))
- [229] Limber D N 1954 The Analysis of Counts of the Extragalactic Nebulae in Terms of a Fluctuating Density Field. II. *Astrophys. J.* **119** 655–+
- [230] Fry J N 1994 Gravity, bias, and the galaxy three-point correlation function *Physical Review Letters* **73** 215–219

- [231] Verde L et al 2002 The 2dF Galaxy Redshift Survey: the bias of galaxies and the density of the Universe *Mon. Not. Roy. Astron. Soc.* **335** 432–440 (*Preprint* [astro-ph/0112161](#))
- [232] Dalal N, Doré O, Huterer D and Shirokov A 2008 Imprints of primordial non-Gaussianities on large-scale structure: Scale-dependent bias and abundance of virialized objects *Phys. Rev. D* **77** 123514 (*Preprint* [0710.4560](#))
- [233] Matarrese S and Verde L 2008 The Effect of Primordial Non-Gaussianity on Halo Bias *Astrophys. J. Lett.* **677** L77–L80 (*Preprint* [0801.4826](#))
- [234] Schneider M, Knox L, Zhan H and Connolly A 2006 Using Galaxy Two-Point Correlation Functions to Determine the Redshift Distributions of Galaxies Binned by Photometric Redshift *Astrophys. J.* **651** 14–23 (*Preprint* [astro-ph/0606098](#))
- [235] Eisenstein D J, Hu W and Tegmark M 1998 Cosmic Complementarity:  $H_0$  and  $\Omega_m$  from Combining Cosmic Microwave Background Experiments and Redshift Surveys *Astrophys. J. Lett.* **504** L57–L60 (*Preprint* [astro-ph/9805239](#))
- [236] Cooray A, Hu W, Huterer D and Joffe M 2001 Measuring Angular Diameter Distances through Halo Clustering *Astrophys. J. Lett.* **557** L7–L10 (*Preprint* [astro-ph/0105061](#))
- [237] Blake C and Glazebrook K 2003 Probing Dark Energy Using Baryonic Oscillations in the Galaxy Power Spectrum as a Cosmological Ruler *Astrophys. J.* **594** 665–673 (*Preprint* [astro-ph/0301632](#))
- [238] Beutler F et al 2011 The 6dF Galaxy Survey: baryon acoustic oscillations and the local Hubble constant *Mon. Not. Roy. Astron. Soc.* **416** 3017–3032 (*Preprint* [1106.3366](#))
- [239] Font-Ribera A et al 2014 Quasar-Lyman  $\alpha$  forest cross-correlation from BOSS DR11: Baryon Acoustic Oscillations *J. Cosmo. Astropart. Phys.* **5** 027 (*Preprint* [1311.1767](#))
- [240] Anderson L et al 2014 The clustering of galaxies in the SDSS-III Baryon Oscillation Spectroscopic Survey: baryon acoustic oscillations in the Data Releases 10 and 11 Galaxy samples *Mon. Not. Roy. Astron. Soc.* **441** 24–62 (*Preprint* [1312.4877](#))
- [241] Delubac T et al 2015 Baryon acoustic oscillations in the Ly $\alpha$  forest of BOSS DR11 quasars *Astron. & Astrophys.* **574** A59 (*Preprint* [1404.1801](#))
- [242] Seo H J, Siegel E R, Eisenstein D J and White M 2008 Nonlinear Structure Formation and the Acoustic Scale *Astrophys. J.* **686** 13–24 (*Preprint* [0805.0117](#))
- [243] Seo H J, Eckel J, Eisenstein D J, Mehta K, Metchnik M, Padmanabhan N, Pinto P, Takahashi R, White M and Xu X 2010 High-precision Predictions for the Acoustic Scale in the Nonlinear Regime *Astrophys. J.* **720** 1650–1667 (*Preprint* [0910.5005](#))
- [244] Sherwin B D and Zaldarriaga M 2012 Shift of the baryon acoustic oscillation scale: A simple physical picture *Phys. Rev. D* **85** 103523 (*Preprint* [1202.3998](#))
- [245] McCullagh N, Neyrinck M C, Szapudi I and Szalay A S 2013 Removing Baryon-acoustic-oscillation Peak Shifts with Local Density Transforms *Astrophys. J. Lett.* **763** L14 (*Preprint* [1211.3130](#))
- [246] Crocce M and Scoccimarro R 2008 Nonlinear evolution of baryon acoustic oscillations *Phys. Rev. D* **77** 023533 (*Preprint* [0704.2783](#))
- [247] Wittman D M, Tyson J A, Kirkman D, Dell’Antonio I and Bernstein G 2000 Detection of weak gravitational lensing distortions of distant galaxies by cosmic dark matter at large scales *Nature* **405** 143–148 (*Preprint* [astro-ph/0003014](#))
- [248] Van Waerbeke L et al 2000 Detection of correlated galaxy ellipticities from CFHT data: first evidence for gravitational lensing by large-scale structures *Astron. & Astrophys.* **358** 30–44 (*Preprint* [astro-ph/0002500](#))

- [249] Bacon D J, Refregier A R and Ellis R S 2000 Detection of weak gravitational lensing by large-scale structure *Mon. Not. Roy. Astron. Soc.* **318** 625–640 (*Preprint* [astro-ph/0003008](#))
- [250] Bartelmann M and Schneider P 2001 Weak gravitational lensing *Phys. Rep.* **340** 291–472 (*Preprint* [astro-ph/9912508](#))
- [251] Munshi D, Valageas P, van Waerbeke L and Heavens A 2008 Cosmology with weak lensing surveys *Phys. Rep.* **462** 67–121 (*Preprint* [astro-ph/0612667](#))
- [252] Mandelbaum R et al 2014 The Third Gravitational Lensing Accuracy Testing (GREAT3) Challenge Handbook *Astrophys. J. Supp.* **212** 5 (*Preprint* [1308.4982](#))
- [253] Schneider M D, Hogg D W, Marshall P J, Dawson W A, Meyers J, Bard D J and Lang D 2015 Hierarchical Probabilistic Inference of Cosmic Shear *Astrophys. J.* **807** 87 (*Preprint* [1411.2608](#))
- [254] Bernstein G M, Armstrong R, Krawiec C and March M C 2016 An accurate and practical method for inference of weak gravitational lensing from galaxy images *Mon. Not. Roy. Astron. Soc.* **459** 4467–4484 (*Preprint* [1508.05655](#))
- [255] Sheldon E S and Huff E M 2017 Practical Weak-lensing Shear Measurement with Metacalibration *Astrophys. J.* **841** 24 (*Preprint* [1702.02601](#))
- [256] Moessner R and Jain B 1998 Angular cross-correlation of galaxies - A probe of gravitational lensing by large-scale structure *Mon. Not. Roy. Astron. Soc.* **294** L18–L24 (*Preprint* [astro-ph/9709159](#))
- [257] Jain B 2002 Magnification Effects as Measures of Large-Scale Structure *Astrophys. J. Lett.* **580** L3–L6 (*Preprint* [astro-ph/0208515](#))
- [258] Zhang P and Pen U L 2006 Precision measurement of cosmic magnification from 21-cm emitting galaxies *Mon. Not. Roy. Astron. Soc.* **367** 169–178 (*Preprint* [astro-ph/0504551](#))
- [259] van Waerbeke L 2010 Shear and magnification: cosmic complementarity *Mon. Not. Roy. Astron. Soc.* **401** 2093–2100 (*Preprint* [0906.1583](#))
- [260] Huterer D, Takada M, Bernstein G and Jain B 2006 Systematic errors in future weak-lensing surveys: requirements and prospects for self-calibration *Mon. Not. Roy. Astron. Soc.* **366** 101–114 (*Preprint* [astro-ph/0506030](#))
- [261] Massey R et al 2013 Origins of weak lensing systematics, and requirements on future instrumentation (or knowledge of instrumentation) *Mon. Not. Roy. Astron. Soc.* **429** 661–678 (*Preprint* [1210.7690](#))
- [262] Jee M J, Tyson J A, Schneider M D, Wittman D, Schmidt S and Hilbert S 2013 Cosmic Shear Results from the Deep Lens Survey. I. Joint Constraints on  $\Omega_M$  and  $\sigma_8$  with a Two-dimensional Analysis *Astrophys. J.* **765** 74 (*Preprint* [1210.2732](#))
- [263] Jee M J, Tyson J A, Hilbert S, Schneider M D, Schmidt S and Wittman D 2016 Cosmic Shear Results from the Deep Lens Survey. II. Full Cosmological Parameter Constraints from Tomography *Astrophys. J.* **824** 77 (*Preprint* [1510.03962](#))
- [264] Chang C et al 2013 Spurious shear in weak lensing with the Large Synoptic Survey Telescope *Mon. Not. Roy. Astron. Soc.* **428** 2695–2713 (*Preprint* [1206.1378](#))
- [265] Petri A, May M, Haiman Z and Kratochvil J M 2014 Impact of spurious shear on cosmological parameter estimates from weak lensing observables *Phys. Rev. D* **90** 123015 (*Preprint* [1409.5130](#))

- [266] Ma Z, Hu W and Huterer D 2006 Effects of Photometric Redshift Uncertainties on Weak-Lensing Tomography *Astrophys. J.* **636** 21–29 (*Preprint* [astro-ph/0506614](#))
- [267] Bernstein G and Huterer D 2010 Catastrophic photometric redshift errors: weak-lensing survey requirements *Mon. Not. Roy. Astron. Soc.* **401** 1399–1408 (*Preprint* [0902.2782](#))
- [268] Hearin A P, Zentner A R, Ma Z and Huterer D 2010 A General Study of the Influence of Catastrophic Photometric Redshift Errors on Cosmology with Cosmic Shear Tomography *Astrophys. J.* **720** 1351–1369 (*Preprint* [1002.3383](#))
- [269] Newman J A 2008 Calibrating Redshift Distributions beyond Spectroscopic Limits with Cross-Correlations *Astrophys. J.* **684** 88–101 (*Preprint* [0805.1409](#))
- [270] Matthews D J and Newman J A 2012 Improving Correlation Function Fitting with Ridge Regression: Application to Cross-correlation Reconstruction *Astrophys. J.* **745** 180 (*Preprint* [1109.2121](#))
- [271] Zhang P, Pen U L and Bernstein G 2010 Self-calibration of photometric redshift scatter in weak-lensing surveys *Mon. Not. Roy. Astron. Soc.* **405** 359–374 (*Preprint* [0910.4181](#))
- [272] Dawson W A, Schneider M D, Tyson J A and Jee M J 2016 The Ellipticity Distribution of Ambiguously Blended Objects *Astrophys. J.* **816** 11 (*Preprint* [1406.1506](#))
- [273] Mandelbaum R *et al* 2018 The first-year shear catalog of the Subaru Hyper Suprime-Cam Subaru Strategic Program Survey *Pub. Astron. Soc. Japan* **70** S25 (*Preprint* [1705.06745](#))
- [274] Catelan P, Kamionkowski M and Blandford R D 2001 Intrinsic and extrinsic galaxy alignment *Mon. Not. Roy. Astron. Soc.* **320** L7–L13 (*Preprint* [astro-ph/0005470](#))
- [275] Hirata C M and Seljak U 2004 Intrinsic alignment-lensing interference as a contaminant of cosmic shear *Phys. Rev. D* **70** 063526 (*Preprint* [astro-ph/0406275](#))
- [276] King L and Schneider P 2002 Suppressing the contribution of intrinsic galaxy alignments to the shear two-point correlation function *Astron. & Astrophys.* **396** 411–418 (*Preprint* [astro-ph/0208256](#))
- [277] King L J 2005 Cosmic shear as a tool for precision cosmology: minimising intrinsic galaxy alignment-lensing interference *Astron. & Astrophys.* **441** 47–53 (*Preprint* [astro-ph/0506441](#))
- [278] Joachimi B and Bridle S L 2010 Simultaneous measurement of cosmology and intrinsic alignments using joint cosmic shear and galaxy number density correlations *Astron. & Astrophys.* **523** A1 (*Preprint* [0911.2454](#))
- [279] Heymans C *et al* 2013 CFHTLenS tomographic weak lensing cosmological parameter constraints: Mitigating the impact of intrinsic galaxy alignments *Mon. Not. Roy. Astron. Soc.* **432** 2433–2453 (*Preprint* [1303.1808](#))
- [280] Troxel M A and Ishak M 2015 The intrinsic alignment of galaxies and its impact on weak gravitational lensing in an era of precision cosmology *Phys. Rep.* **558** 1–59 (*Preprint* [1407.6990](#))
- [281] Krause E and Eifler T 2017 cosmolike - cosmological likelihood analyses for photometric galaxy surveys *Mon. Not. Roy. Astron. Soc.* **470** 2100–2112 (*Preprint* [1601.05779](#))
- [282] Mandelbaum R *et al* 2011 The WiggleZ Dark Energy Survey: direct constraints on blue galaxy intrinsic alignments at intermediate redshifts *Mon. Not. Roy. Astron. Soc.* **410** 844–859 (*Preprint* [0911.5347](#))

- [283] Broadhurst T J, Taylor A N and Peacock J A 1995 Mapping cluster mass distributions via gravitational lensing of background galaxies *Astrophys. J.* **438** 49–61 (*Preprint* [astro-ph/9406052](#))
- [284] Tyson J A 1988 Deep CCD survey - Galaxy luminosity and color evolution *Astron. J.* **96** 1–23
- [285] Yang X, Zhang P, Zhang J and Yu Y 2015 Weak lensing reconstruction through cosmic magnification - II. Improved power spectrum determination and map-making *Mon. Not. Roy. Astron. Soc.* **447** 345–362 (*Preprint* [1309.2474](#))
- [286] Yang X and Zhang P 2011 Weak lensing reconstruction through cosmic magnification - I. A minimal variance map reconstruction *Mon. Not. Roy. Astron. Soc.* **415** 3485–3496 (*Preprint* [1105.2385](#))
- [287] Morrison C B, Scranton R, Ménard B, Schmidt S J, Tyson J A, Ryan R, Choi A and Wittman D M 2012 Tomographic magnification of Lyman-break galaxies in the Deep Lens Survey *Mon. Not. Roy. Astron. Soc.* **426** 2489–2499 (*Preprint* [1204.2830](#))
- [288] Phillips M M 1993 The absolute magnitudes of Type IA supernovae *Astrophys. J. Lett.* **413** L105–L108
- [289] Jha S, Riess A G and Kirshner R P 2007 Improved Distances to Type Ia Supernovae with Multicolor Light-Curve Shapes: MLCS2k2 *Astrophys. J.* **659** 122–148 (*Preprint* [astro-ph/0612666](#))
- [290] Guy J *et al* 2007 SALT2: using distant supernovae to improve the use of type Ia supernovae as distance indicators *Astron. & Astrophys.* **466** 11–21 (*Preprint* [astro-ph/0701828](#))
- [291] Conley A *et al* 2008 SiFTO: An Empirical Method for Fitting SN Ia Light Curves *Astrophys. J.* **681** 482–498 (*Preprint* [0803.3441](#))
- [292] Wood-Vasey W M *et al* 2008 Type Ia Supernovae Are Good Standard Candles in the Near Infrared: Evidence from PAIRITEL *Astrophys. J.* **689** 377–390 (*Preprint* [0711.2068](#))
- [293] Barone-Nugent R L *et al* 2012 Near-infrared observations of Type Ia supernovae: the best known standard candle for cosmology *Mon. Not. Roy. Astron. Soc.* **425** 1007–1012 (*Preprint* [1204.2308](#))
- [294] Sullivan M *et al* 2006 Photometric Selection of High-Redshift Type Ia Supernova Candidates *Astron. J.* **131** 960–972 (*Preprint* [astro-ph/0510857](#))
- [295] Sako M *et al* 2011 Photometric Type Ia Supernova Candidates from the Three-year SDSS-II SN Survey Data *Astrophys. J.* **738** 162 (*Preprint* [1107.5106](#))
- [296] Zentner A R and Bhattacharya S 2009 Utilizing Type Ia Supernovae in a Large, Fast, Imaging Survey to Constrain Dark Energy *Astrophys. J.* **693** 1543–1553 (*Preprint* [0812.0358](#))
- [297] Allen S W, Evrard A E and Mantz A B 2011 Cosmological Parameters from Observations of Galaxy Clusters *Ann. Rev. Astron. & Astrophys.* **49** 409–470 (*Preprint* [1103.4829](#))
- [298] Press W H and Schechter P 1974 Formation of Galaxies and Clusters of Galaxies by Self-Similar Gravitational Condensation *Astrophys. J.* **187** 425–438
- [299] Bond J R, Cole S, Efstathiou G and Kaiser N 1991 Excursion set mass functions for hierarchical Gaussian fluctuations *Astrophys. J.* **379** 440–460

- [300] Jenkins A, Frenk C S, White S D M, Colberg J M, Cole S, Evrard A E, Couchman H M P and Yoshida N 2001 The mass function of dark matter haloes *Mon. Not. Roy. Astron. Soc.* **321** 372–384 (*Preprint* [astro-ph/0005260](#))
- [301] Tinker J, Kravtsov A V, Klypin A, Abazajian K, Warren M, Yepes G, Gottlöber S and Holz D E 2008 Toward a Halo Mass Function for Precision Cosmology: The Limits of Universality *Astrophys. J.* **688** 709–728 (*Preprint* [0803.2706](#))
- [302] Haiman Z, Mohr J J and Holder G P 2001 Constraints on Cosmological Parameters from Future Galaxy Cluster Surveys *Astrophys. J.* **553** 545–561 (*Preprint* [astro-ph/0002336](#))
- [303] Majumdar S and Mohr J J 2004 Self-Calibration in Cluster Studies of Dark Energy: Combining the Cluster Redshift Distribution, the Power Spectrum, and Mass Measurements *Astrophys. J.* **613** 41–50 (*Preprint* [astro-ph/0305341](#))
- [304] Rozo E et al 2010 Cosmological Constraints from the Sloan Digital Sky Survey maxBCG Cluster Catalog *Astrophys. J.* **708** 645–660 (*Preprint* [0902.3702](#))
- [305] Lima M and Hu W 2005 Self-calibration of cluster dark energy studies: Observable-mass distribution *Phys. Rev. D* **72** 043006 (*Preprint* [astro-ph/0503363](#))
- [306] Frenk C S et al 1999 The Santa Barbara Cluster Comparison Project: A Comparison of Cosmological Hydrodynamics Solutions *Astrophys. J.* **525** 554–582 (*Preprint* [astro-ph/9906160](#))
- [307] Nagai D, Vikhlinin A and Kravtsov A V 2007 Testing X-Ray Measurements of Galaxy Clusters with Cosmological Simulations *Astrophys. J.* **655** 98–108 (*Preprint* [astro-ph/0609247](#))
- [308] Kravtsov A V and Borgani S 2012 Formation of Galaxy Clusters *Ann. Rev. Astron. & Astrophys.* **50** 353–409 (*Preprint* [1205.5556](#))
- [309] Becker M R and Kravtsov A V 2011 On the Accuracy of Weak-lensing Cluster Mass Reconstructions *Astrophys. J.* **740** 25 (*Preprint* [1011.1681](#))
- [310] Wu H Y, Rozo E and Wechsler R H 2010 Annealing a Follow-up Program: Improvement of the Dark Energy Figure of Merit for Optical Galaxy Cluster Surveys *Astrophys. J.* **713** 1207–1218 (*Preprint* [0907.2690](#))
- [311] Mantz A, Allen S W, Ebeling H, Rapetti D and Drlica-Wagner A 2010 The observed growth of massive galaxy clusters - II. X-ray scaling relations *Mon. Not. Roy. Astron. Soc.* **406** 1773–1795 (*Preprint* [0909.3099](#))
- [312] Colley W N, Tyson J A and Turner E L 1996 Unlensing Multiple Arcs in 0024+1654: Reconstruction of the Source Image *Astrophys. J. Lett.* **461** L83 (*Preprint* [astro-ph/9512128](#))
- [313] Inada N et al 2003 A gravitationally lensed quasar with quadruple images separated by 14.62arcseconds *Nature* **426** 810–812 (*Preprint* [astro-ph/0312427](#))
- [314] King L J et al 1998 A complete infrared Einstein ring in the gravitational lens system B1938 + 666 *Mon. Not. Roy. Astron. Soc.* **295** L41 (*Preprint* [astro-ph/9710171](#))
- [315] Kelly P L et al 2015 Multiple images of a highly magnified supernova formed by an early-type cluster galaxy lens *Science* **347** 1123–1126 (*Preprint* [1411.6009](#))
- [316] Goobar A et al 2017 iPTF16geu: A multiply imaged, gravitationally lensed type Ia supernova *Science* **356** 291–295 (*Preprint* [1611.00014](#))
- [317] Refsdal S 1964 On the possibility of determining Hubble’s parameter and the masses of galaxies from the gravitational lens effect *Mon. Not. Roy. Astron. Soc.* **128** 307

- [318] Suyu S H, Marshall P J, Auger M W, Hilbert S, Blandford R D, Koopmans L V E, Fassnacht C D and Treu T 2010 Dissecting the Gravitational lens B1608+656. II. Precision Measurements of the Hubble Constant, Spatial Curvature, and the Dark Energy Equation of State *Astrophys. J.* **711** 201–221 (*Preprint* [0910.2773](#))
- [319] Linder E V 2011 Lensing time delays and cosmological complementarity *Phys. Rev. D* **84** 123529 (*Preprint* [1109.2592](#))
- [320] Oguri M and Marshall P J 2010 Gravitationally lensed quasars and supernovae in future wide-field optical imaging surveys *Mon. Not. Roy. Astron. Soc.* **405** 2579–2593 (*Preprint* [1001.2037](#))
- [321] Gavazzi R, Treu T, Koopmans L V E, Bolton A S, Moustakas L A, Burles S and Marshall P J 2008 The Sloan Lens ACS Survey. VI. Discovery and Analysis of a Double Einstein Ring *Astrophys. J.* **677** 1046–1059 (*Preprint* [0801.1555](#))
- [322] Jullo E, Natarajan P, Kneib J P, D’Aloisio A, Limousin M, Richard J and Schimd C 2010 Cosmological Constraints from Strong Gravitational Lensing in Clusters of Galaxies *Science* **329** 924–927 (*Preprint* [1008.4802](#))
- [323] Collett T E and Auger M W 2014 Cosmological constraints from the double source plane lens SDSSJ0946+1006 *Mon. Not. Roy. Astron. Soc.* **443** 969–976 (*Preprint* [1403.5278](#))
- [324] Bernstein G M 2009 Comprehensive Two-Point Analyses of Weak Gravitational Lensing Surveys *Astrophys. J.* **695** 652–665 (*Preprint* [0808.3400](#))
- [325] Mandelbaum R, Slosar A, Baldauf T, Seljak U, Hirata C M, Nakajima R, Reyes R and Smith R E 2013 Cosmological parameter constraints from galaxy-galaxy lensing and galaxy clustering with the SDSS DR7 *Mon. Not. Roy. Astron. Soc.* **432** 1544–1575 (*Preprint* [1207.1120](#))
- [326] Zhan H *et al* 2009 Exploring Dark Energy with Next-Generation Photometric Redshift Surveys *astro2010: The Astronomy and Astrophysics Decadal Survey (Astronomy vol 2010)* (*Preprint* [0902.2599](#))
- [327] Jungman G, Kamionkowski M, Kosowsky A and Spergel D N 1996 Cosmological-parameter determination with microwave background maps *Phys. Rev. D* **54** 1332–1344 (*Preprint* [astro-ph/9512139](#))
- [328] Tegmark M, Taylor A N and Heavens A F 1997 Karhunen-Loève Eigenvalue Problems in Cosmology: How Should We Tackle Large Data Sets? *Astrophys. J.* **480** 22–35 (*Preprint* [astro-ph/9603021](#))
- [329] van Uitert E *et al* 2017 KiDS+GAMA: Cosmology constraints from a joint analysis of cosmic shear, galaxy-galaxy lensing and angular clustering *ArXiv e-prints* (*Preprint* [1706.05004](#))
- [330] Planck Collaboration: Aghanim N *et al* 2016 Planck 2015 results. XI. CMB power spectra, likelihoods, and robustness of parameters *Astron. & Astrophys.* **594** A11 (*Preprint* [1507.02704](#))
- [331] Goodman J and Weare J 2010 Ensemble samplers with affine invariance *Comm. App. Math. Comp. Sci.* **5** 65–80
- [332] Xu Y, Zhan H and Cheung Y K E 2017 Reconstructing the Cosmic Expansion History with a Monotonicity Prior *ArXiv e-prints* (*Preprint* [1710.02947](#))
- [333] Palanque-Delabrouille N *et al* 2010 Photometric redshifts for type Ia supernovae in the supernova legacy survey *Astron. & Astrophys.* **514** A63 (*Preprint* [0911.1629](#))

- [334] Kessler R *et al* 2010 Photometric Estimates of Redshifts and Distance Moduli for Type Ia Supernovae *Astrophys. J.* **717** 40–57 (*Preprint* [1001.0738](#))
- [335] Wang Y, Gjergo E and Kuhlmann S 2015 Analytic photometric redshift estimator for Type Ia supernovae from the Large Synoptic Survey Telescope *Mon. Not. Roy. Astron. Soc.* **451** 1955–1963 (*Preprint* [1501.06839](#))
- [336] Astier P *et al* 2006 The Supernova Legacy Survey: measurement of  $\Omega_M$ ,  $\Omega$  and  $w$  from the first year data set *Astron. & Astrophys.* **447** 31–48 (*Preprint* [astro-ph/0510447](#))
- [337] Barnard M, Abrahamse A, Albrecht A, Bozek B and Yashar M 2008 Measure of the impact of future dark energy experiments based on discriminating power among quintessence models *Phys. Rev. D* **78** 043528 (*Preprint* [0804.0413](#))
- [338] URL <http://sci.esa.int/euclid/>
- [339] URL <https://wfirst.gsfc.nasa.gov/>
- [340] Harrison F A *et al* 2013 The Nuclear Spectroscopic Telescope Array (NuSTAR) High-energy X-Ray Mission *Astrophys. J.* **770** 103 (*Preprint* [1301.7307](#))
- [341] Atwood W B *et al* 2009 The Large Area Telescope on the Fermi Gamma-Ray Space Telescope Mission *Astrophys. J.* **697** 1071–1102 (*Preprint* [0902.1089](#))
- [342] Gardner J P *et al* 2006 The James Webb Space Telescope *Space Sci. Rev.* **123** 485–606 (*Preprint* [astro-ph/0606175](#))
- [343] URL <http://www.gmto.org/>
- [344] URL <http://www.tmt.org/>
- [345] URL <http://www.eso.org/public/teles-instr/e-elt/>
- [346] URL <http://skatelescope.org/>
- [347] B Jain *et al* 2015 The Whole is Greater than the Sum of the Parts: Optimizing the Joint Science Return from LSST, Euclid and WFIRST *ArXiv e-prints* (*Preprint* [1501.07897](#))